Insulin potentiates the synchronous firing of arcuate nucleus Kiss1 neurons that protects against diet-induced obesity

Jian Qiu[a], Todd L. Stincic[a], Martha A. Bosch[a], Ashley M. Connors[a], Stefanie Kaech Petrie [b], Oline K. Rønnekleiv[a,c], Martin J. Kelly[a,c]

[a]Department of Chemical Physiology and Biochemistry, Oregon Health and Science University, Portland, United States

[b]Jungers Center for Neurosciences Research, Oregon Health and Science University, Portland, United States

[c]Division of Neuroscience, Oregon National Primate Research Center, Oregon Health and Science University, Beaverton, United States

Short Title: Insulin potentiates the synchronous activity of arcuate Kiss1 neurons

Co-corresponding Authors:
Jian Qiu, Ph.D. and Martin J. Kelly, Ph.D.
Department of Chemical Physiology and Biochemistry
Oregon Health and Science University
3181 SW Sam Jackson Park Road
Portland, Oregon, 97239, United States
Tel: 503-494-5835
E-mail: giuj@ohsu.edu or kellym@ohsu.edu

Number of Tables: 1
Number of Figures: 8
Word count: 7,580
Keywords: KNDy neurons, slow EPSP, insulin, TRPC5 channel, stromal interaction molecule 1

Abstract

Kisspeptin neurons in the hypothalamic arcuate nucleus (Kiss1^{ARH}) co-express kisspeptin, neurokinin B, dynorphin and provide an episodic, excitatory drive to gonadotropin-releasing hormone (GnRH) neurons, which is critical for pubertal development and fertility. Previously, we showed that high frequency firing of Kiss1^{ARH} neurons co-releases NKB and dynorphin onto neighboring Kiss1^{ARH} neurons to generate a slow excitatory postsynaptic potential (EPSP) that entrains intermittent, synchronous firing of Kiss1^{ARH} neurons (Qiu et al., 2016). Presently, we discovered that insulin significantly increased the amplitude of the slow EPSP, which we documented is mediated by TRPC5 channels, and augmented synchronous GCaMP6s ($[Ca]_i$) oscillations in Kiss1^{ARH} neurons. Deletion of the endoplasmic reticulum calcium-sensing protein stromal interaction molecule 1 in Kiss1^{ARH} neurons amplified insulin's actions and protected ovariectomized female mice from developing obesity and glucose intolerance with high-fat dieting. Therefore, insulin appears to be critical for facilitating synchronous firing of Kiss1^{ARH} neurons and coordinating energy homeostasis with fertility.

Introduction

Multi-unit recordings first done in female rhesus macaques identified synchronous volleys of action potentials in the hypothalamic arcuate nucleus that correlated with pulsatile luteinizing hormone (LH) release (Knobil, 1981; Wilson et al., 1984). It was later proposed that hypothalamic arcuate kisspeptin (Kiss1^{ARH}) neurons were responsible for the "pulse-generator" activity that stimulates pulsatile secretion of gonadotropin releasing hormone (GnRH) and subsequently LH (Lehman et al., 2010; Navarro V. M. et al., 2009), and multi-unit recordings targeting these neurons supported this hypothesis (Kinsey-Jones et al., 2008; Okamura et al., 2013). Indeed, recent experiments showed that high frequency optogenetic stimulation of Kiss1^{ARH} neurons expressing channel rhodopsin (ChR2) generates pulsatile release of LH (Clarkson et al., 2017), and we elucidated the cellular mechanism responsible for synchronizing the "pulse generator" Kiss1^{ARH} neurons (Qiu J. et al., 2016). Key to the synchronous firing of thousands of Kiss1^{ARH} neurons is the fact that these neurons co-express neurokinin B (NKB) and dynorphin (Goodman et al., 2007), and high-frequency firing of Kiss1^{ARH} neurons co-

releases NKB and dynorphin (Qiu J. et al., 2016). NKB binds to tachykinin 3 receptor (TacR3) in neighboring Kiss1^{ARH} neurons to activate canonical transient receptor potential 5 (TRPC5) channels to cause a robust depolarization (slow EPSP), whereas co-released dynorphin feeds back to bind to presynaptic κ-opioid receptors to limit the release of NKB to discrete bursts of activity (Qiu J. et al., 2016). The co-release of the two peptide neurotransmitters coordinates the synchronous firing of Kiss1^{ARH} neurons that drives the pulsatile release of GnRH into the median eminence (Clarkson et al., 2017; Qiu J. et al., 2016). This mode of synchronization appears to be quite different than what has been reported for organotypic cultures of immature kisspeptin neurons where the peptides have a modest effect on Ca^{2+} oscillations (Kim et al., 2020).

The metabolic hormones leptin and insulin excite/depolarize Kiss1^{ARH}, and proopiomelanocortin (POMC), neurons through activation of TRPC5 channels (Kelly Martin J. et al., 2018; Qiu J. et al., 2011; Qiu J. et al., 2010; Qiu J. et al., 2014). In contrast, leptin and insulin inhibit/hyperpolarizes neuropeptide Y/agouti-related peptide (NPY/AgRP) neurons via activation of K_{ATP} channels (Qiu J. et al., 2020; Qiu J., Wagner, et al., 2018; Qiu J. et al., 2014). The excitatory actions of leptin and insulin on Kiss1^{ARH} and POMC neurons and inhibitory actions on NPY/AgRP neurons are complementary for mediating the anorexigenic effects of these metabolic hormones (Stincic et al., 2019). The increase in POMC and Kiss1^{ARH} cell excitability induced by insulin translates into heightened transcriptional activity—*i.e.,* an increase in c-Fos expression in the arcuate nucleus following *icv* insulin (Qiu J. et al., 2014). Insulin delivered directly into the third ventricle uniformly decreases food intake in guinea pigs (Qiu J. et al., 2014), mice (Benoit et al., 2002; Brown et al., 2006) and rats (Clegg et al., 2011), which correlates with alterations in energy expenditure as manifested by increases in O_2 consumption, CO_2 production and metabolic heat production (Qiu J. et al., 2014). Optogenetic and pharmacogenetic stimulation of NPY/AgRP neurons rapidly increases food consumption (Aponte et al., 2011; Krashes et al., 2011), but stimulation of POMC neurons attenuates food intake (Aponte et al., 2011; Wei et al., 2018). Moreover, toxin-induced silencing of the "anorexigenic" Kiss1^{ARH} neurons in females creates an obese phenotype (Padilla et al., 2019). The cumulative effects of leptin and insulin in ARH neurons are vital for both the short term (excitability) and long-term (transcriptional) modulation of neuronal activity and the control of food intake and ultimately energy homeostasis.

In POMC neurons the insulin receptor (InsR) couples to phosphoinositide 3-kinase (PI3K) p110β activation (Al-Qassab et al., 2009; Xu et al., 2005), and the InsR-mediated excitation of POMC neurons is abrogated by inhibition of PI3K activity (Al-Qassab et al., 2009; Hill et al., 2008; Qiu J. et al., 2010; Qiu J. et al., 2014). In $Kiss1^{ARH}$ neurons leptin signals via PI3K to activate TRPC5 channels (Qiu J. et al., 2011), and insulin has similar effects (Qiu J. et al., 2014). Activation of PI3K generates PIP_3, which stimulates phospholipase C (PLC) and protein kinase B (Akt) (Bae et al., 1998; Falasca et al., 1998; Qiu J. et al., 2014; Rameh et al., 1998). PLC also hydrolyzes PIP_2, which modulates TRPC4, 5 channel activity (Qiu J. et al., 2014; Rodríguez-Menchaca et al., 2012; Zhang, Bosch, et al., 2013). In addition, PI3K rapidly increases the insertion of TRPC5 channels into the plasma membrane from vesicular pools held in reserve beneath the membrane (Bezzerides et al., 2004). The increase in TRPC5 channel availability further boosts depolarization and Ca^{2+} entry into neurons. Collectively, all of these PI3K-mediated effects are critically involved in the activation of TRPC5 channels by insulin actions in POMC, and presumably Kiss1 neurons (Qiu J., Bosch, et al., 2018).

A key molecule modulating the activity of TRPC channels is stromal-interaction molecule 1 (STIM1), which is localized to the endoplasmic reticulum (ER) membrane of cells, and its N-terminal domain contains an EF-hand that protrudes into the lumen of the ER to sense changes in ER Ca^{2+} concentrations and maintain intracellular Ca^{2+} homeostasis through store-operated Ca^{2+} entry (SOCE) (Salido et al., 2011). Upon depletion of endoplasmic reticulum Ca^{2+}, STIM1 undergoes a conformational change, oligomerizes and then interacts with plasma membrane calcium channels, including TRPC channels (Salido et al., 2011; Yuan et al., 2007). Under normal physiological conditions, TRPC5 channels are coupled to plasma membrane receptors (insulin receptor, leptin receptor, serotonin $5HT_{2C}$ receptor) (Gao et al., 2017; Qiu J. et al., 2010; Qiu J. et al., 2014), but in cellular stressed states (*e.g.,* obesity) it is thought that TRPC5 channels associate with STIM1 to replete endoplasmic reticulum Ca^{2+} stores (Birnbaumer, 2009; Qiu J., Bosch, et al., 2018). We found that in POMC neurons estradiol protects against insulin resistance by downregulating *Stim1* expression and thereby maintaining the excitatory effects of insulin in obese females (Qiu J., Bosch, et al., 2018). Therefore, in the present study we generated $Kiss1^{Cre}::Stim1^{lox/lox}$ mice to study the consequences of deletion of STIM1 on insulin's effects in $Kiss1^{ARH}$ neurons and ultimately its facilitatory effects on synchronization of pulse generator activity.

Results

Validation of conditional deletion of Stim1 in Kiss1 neurons

STIM1 is involved in the regulation of neuronal firing in cerebellar Purkinje neurons (Hartmann et al., 2014; Ryu et al., 2017), dopaminergic neurons (Sun et al., 2017) and hypothalamic arcuate POMC neurons (Qiu J., Bosch, et al., 2018). First, to see if STIM1 regulates $Kiss1^{ARH}$ neuronal excitability, we determined mRNA expression of *Stim1* and its close homolog *Stim2* in manually harvested $Kiss1^{ARH}$ neurons by quantitative real-time PCR (***Figure 1A***). Based on the qPCR, mRNA levels of *Stim1* were greater than those of *Stim2* in $Kiss1^{ARH}$ neurons (***Figure 1A****, left panel*). Likewise, in cerebellar Purkinje neurons, *Stim1* is also much more abundant than *Stim2* (Hartmann et al., 2014), while in hippocampal (Berna-Erro et al., 2009) and cortical neurons (Gruszczynska-Biegala et al., 2011) *Stim2* expression levels exceed those of *Stim1*. A qualitative, unbiased sampling of $Kiss1^{ARH}$ neurons (n=60) from ovariectomized $Kiss1^{Cre}$ females (n =3) revealed that *Stim1* mRNA was expressed in 81.7 ± 7.6 percent and *Stim2* mRNA was detected in 81.2 ± 2.7 percentage of $Kiss1^{ARH}$ neurons with 70 percentage expressing both *Stim1* and *Stim2*.

To elucidate the functional role of STIM1 in Kiss1 neurons, we generated mice that lack STIM1 selectively in Kiss1 neurons ($Stim1^{kko}$, detailed in Methods). We confirmed the *Stim1* deletion in $Stim1^{kko}$ mice using single cell quantitative PCR of pools of harvested $Kiss1^{ARH}$ neurons (n= 3 animals) (***Figure 1A****, middle*). Consistent with the scRT-PCR results (***Figure 1B***), *Stim1* mRNA was undetectable in $Stim1^{kko}$ neurons (***Figure 1A****, middle*), whereas there were no reduction in *Stim2* mRNA expression (***Figure 1A****, right*).

Previous results show that insulin receptor (*Insr*) and *Trpc5* mRNA are expressed and involved in sculpting the excitability in $Kiss1^{ARH}$ neurons (Qiu J. et al., 2011; Qiu X. et al., 2013), and insulin excites $Kiss1^{ARH}$ neurons through activation of TPRC5 channels (Qiu J. et al., 2014). To see if *Insr* and *Trpc5* mRNAs are co-localized in $Kiss1^{ARH}$ neurons, we harvested 64 $Kiss1^{ARH}$ neurons from 3 females and did scRT-PCR for *Insr* and Trpc5

(***Figure 1C***). The single-cell analysis revealed that *Insr* transcript was detected in 53% of Kiss1^{ARH} neurons and *Trpc5* mRNA was found in 69% of neurons. Among *Trpc5*-positive Kiss1^{ARH} neurons, 82% expressed *Insr* mRNA.

Stim1 deletion reduces Store Operated Calcium Entry (SOCE)

SOCE constitutes an important source of calcium entry and signaling in neurons. Depletion of ER Ca^{2+} stores causes the ER Ca^{2+} sensor STIM proteins (STIM1 and STIM2) to interact with and activate cell surface Ca^{2+} release-activated Ca^{2+} (CRAC) channels, thereby resulting in a second wave of cytoplasmic Ca^{2+} rise (Moccia et al., 2015). Genetic suppression of *Stim1* in neural progenitor cells results in abrogation of this second wave of calcium rise that constitutes SOCE (Somasundaram et al., 2014). We asked whether deletion of *Stim1* in Kiss1^{ARH} neurons (*Stim1^{kko}*) attenuates neuronal SOCE. We transfected Kiss1^{ARH} or *Stim1^{kko}* neurons with GCaMP6s and imaged these neurons using spinning disk confocal microscopy (***Figure 2-video supplement 1***). ER Ca^{2+} stores were released by treatment with 2 μM thapsigargin (Tg), a blocker of the SERCA (sarcoplasmic/endoplasmic reticulum Ca^{2+} ATPase) pump. As expected, Tg treatment of neurons bathed in Ca^{2+}-free aCSF generated an initial wave of cytoplasmic Ca^{2+} release ($[Ca^{2+}]_i$) as measured by an increase in GCaMP6s activity both in control and *Stim1*-deleted neurons (***Figure 1D, E and F***). As long as neurons were kept in Ca^{2+}- free aCSF, the ER stores remained empty, a situation that was presumably sensed by the Ca^{2+} sensor STIMs. Upon switching to a normal aCSF containing 2 mM Ca^{2+}, an immediate SOCE response was observed as a second wave of cytoplasmic Ca^{2+} rise. Consistent with a role for STIM1 regulation, we observed an attenuation of SOCE in *Stim1^{kko}* neurons (***Figure 1D, E F and G***: $\Delta F/F_0$*100 =1274.5 ± 49.4, n = 4, Kiss1^{ARH} group versus 389.0 ± 86.1, n = 4, Stim1^{kko} group, which was measured from the 15 minute time point to the peak, unpaired t-test, $t_{(6)}$ = 8.921, p = 0.0001, ***p < 0.005), indicating that STIM1 plays a major role in SOCE after Tg-induced ER Ca^{2+} depletion in Kiss1^{ARH} neurons as has been shown in other CNS neurons (Guner et al., 2017; Pavez et al., 2019).

TacR3 -induced increase in $[Ca^{2+}]_i$ is augmented by deletion of Stim1

TacR3 classically couples to a Gαq protein and excites Kiss1^{ARH} neurons (Ruka et al., 2013) (de Croft et al., 2013) (Qiu J. et al., 2016). Calcium is of critical importance to neurons as it participates in the transmission of depolarizing signals and contributes to synaptic activity (Brini et al., 2014). Therefore, we tested whether STIM1 can modulate TacR3-mediated calcium responses. We first measured the effects of the TacR3 agonist senktide on GCaMP6s-expressing Kiss1^{ARH} neurons in arcuate slices from Kiss1^{Cre} mice; senktide (1 μM) rapidly induced an increase in $[Ca^{2+}]_i$ (***Figure 2A and C***). Next, we investigated if STIM1 protein contributes to $[Ca^{2+}]_i$ in neurons after senktide activation from *Stim1^{kko}* mice; deletion of *Stim1* significantly augmented senktide responses (***Figure 2 E and G)***. $\Delta F/F_0*100$ = 236.5 ± 32.7, n = 5, Kiss1^{ARH} group versus 622.1 ± 133.2, n = 6, *Stim1^{kko}* group at the 4 minute time point, unpaired t-test, $t_{(11)}$ = 2.568, *p = 0.0303 (***Figure 2C versus 2G***).

Insulin augments the TacR3-mediated $[Ca^{2+}]_I$ increase

Given that insulin excites Kiss1^{ARH} neurons (Qiu J. et al., 2014), we hypothesized that insulin would also potentiate TacR3-mediated $[Ca^{2+}]_i$ increase. We perfused slices with insulin (20 nM) for 20 minutes, then administered a bolus of senktide directly into the recording chamber. We observed that the increase in peak $[Ca^{2+}]_i$ was augmented by insulin in GCaMP6s-expressing Kiss1^{ARH} neurons from *Kiss1^{Cre}* and *Stim1^{kko}* mice (***Figure 2C and G***). The area under the curve was significantly different in the Kiss1^{ARH} group similar to the *Stim1^{kko}* group comparing with and without pretreatment of insulin (***Figure 2D and H***).

Deletion of STIM1 enhances slow EPSP in Kiss1^{ARH} neurons

Kiss1^{ARH} neurons are the chief component of the GnRH pulse generator circuit (Lehman et al., 2010; Navarro V.M. et al., 2011; Navarro V. M. et al., 2009; Okamura et al., 2013), such that they synchronize their activity to trigger the release of peptides to drive pulsatile release of GnRH (Clarkson et al., 2017; Qiu J. et al., 2016). To investigate if STIM1 proteins modulate the activity of Kiss1^{ARH} neurons, we bilaterally injected AAV1-Ef1a-DIO-

ChR2:mCherry into the arcuate nucleus of *Kiss1*^{Cre} and *Stim1*^{kko} mice (***Figure 3A***), and did whole-cell recordings of Kiss1^{ARH} neurons expressing ChR2-mCherry in slices following photostimulation at 20 Hz for 10 s (***Figure 3-video supplement 1***) as previously described (Qiu J. et al., 2016). As we hypothesized, deletion of *Stim1* augmented the slow EPSP induced by high-frequency optogenetic stimulation (***Figure 3B-D***). Even in the presence of TTX to block voltage-gated Na^+ channels, we still saw that senktide induced larger inward currents in Kiss1^{ARH} neurons from *Stim1*^{kko} mice versus *Kiss1*^{Cre} mice (***Figure 3E-G***).

Effects of insulin are mediated by increased TRPC5 channel activity

PI3K is essential for mediating the effects of insulin (Qiu J. et al., 2014), and it is also critical for the trafficking of TRPC channels (Bezzerides et al., 2004). Therefore, we examined the role of PI3K in the insulin potentiation of the slow EPSP. To exclude the variability from the viral injections, we used *Kiss1*^{Cre}*::Ai32* mice in which all EYFP neurons express *Kiss1* and ChR2 (see Methods). As expected, the selective PI3K inhibitor wortmannin (100 nM) robustly blocked the potentiation of the slow EPSP by insulin (***Figure 4A-E***). Next, we investigated a downstream effector of PI3K signaling based on our previous findings that TPRC5 channel protein is expressed in Kiss1^{ARH} neurons (***Figure 1C***) (Qiu J. et al., 2011) and is activated by the NKB agonist senktide (Kelly Martin J. et al., 2018). To measure the TRPC5 channels contribution to the slow EPSP, we used a ratio method in which a slow EPSP was generated with optogenetic stimulation (20 Hz, 10 s) of a Kiss1^{Cre}:ChR2 neuron and then tested again 10 min later after drug exposure (Qiu J. et al., 2016). Using this protocol, we found that the slow EPSP was inhibited by perfusing the TRPC4/5 channel blocker HC 070 (100 nM) (Just et al., 2018) for 5 mins, and the ratio was significantly decreased from 60 to 30 percent (***Figure 4F-H***). Since *Trpc4* mRNA is not expressed in Kiss1^{ARH} neurons (Bosch et al., *unpublished data*), we would conclude that TRPC5 channels are mediating the slow EPSP in these neurons.

Insulin augments the slow EPSP in Stim1^{kko} *neurons*

To test the hypothesis that insulin potentiates the slow EPSP in *Stim1*^{kko} neurons to a greater extent than in

Kiss1^{ARH} neurons, we pretreated ChR2-mCherry expressing arcuate slices from *Stim1^{kko}* mice with insulin. Indeed, we found that insulin augmented the slow EPSP by 60% beyond the effects of *Stim1* deletion on the slow EPSP. The TRPC5 channel blocker HC 070 (100 nM) reversed the effects of insulin indicating that the effects were mediated by increased TRPC5 channel activity ***(Figure 5A-D)***.

To elucidate the TRPC5 channel contribution to the postsynaptic activity of Kiss1^{ARH} neurons, we perfused TTX to block fast sodium channels and found that HC 070 significantly suppressed the senktide-induced inward current (***Figure 5E, F and H***). The I/V plot for the senktide-induced cation current exhibited the typical double-rectifying characteristics of TRPC5 channels with a reversal of -10 mV (***Figure 5G***) as we previously reported (Kelly Martin J. et al., 2018). These results indicate that TRPC5 channels also contribute to the synchronous activity of *Stim1^{kko}* neurons.

Stim1 deletion in Kiss1^{ARH} neurons protects ovariectomized females against diet-induced obesity

Two cohorts of female mice, *Stim1^{kko}* (n=10) and the littermate control *Kiss1^{Cre}* (n=10) mice, were ovariectomized at 2-4 months of age and put on a high fat diet for eight weeks (see Methods). There was significantly less gain in body weight in the *Stim1^{kko}* versus the *Kiss1^{Cre}* mice (***Figure 6A, B***). Moreover, the average fat mass of *Stim1^{kko}* mice was significantly less that of *Kiss1^{Cre}* controls by week 6 (*Stim1^{kko}* versus *Kiss1^{Cre}* mice: 7.6 ± 0.9 g, n=10 versus 11.4 ± 1.1 g, n=10) (***Figure 6C***). The lean mass of *Stim1^{kko}* mice was significantly less versus the *Kiss1^{Cre}* mice (*Stim1^{kko}* versus the *Kiss1^{Cre}* mice: 16.9 ± 0.4 g, n=10 versus 18.9 ± 0.4 g, n=10) (***Figure 6D***). After 6 weeks, both *Stim1^{kko}* and *Kiss1^{Cre}* controls were assessed for glucose tolerance using an *i.p*. glucose tolerance test (see Methods). Both *Stim1^{kko}* and *Kiss1^{Cre}* females started at relatively the same blood glucose levels after an overnight fast (***Figure 6E*****,** *time 0*), suggesting similar whole-body homeostatic conditions after fasting. However, *Stim1^{kko}* female mice had significantly lower glucose levels after *i.p.* glucose compared to *Kiss1^{Cre}* females, indicating that *Stim1^{kko}* females were more glucose tolerant compared to *Kiss1^{Cre}* controls. Moreover, *Stim1^{kko}* females had a significantly different glucose clearance rate than controls based on the integrated area under the curve (*Stim1^{kko}* versus the *Kiss1^{Cre}* controls AUC: 20,232 ± 868 mg/dL × min, n =

6 vs 22,622 ± 624 mg/dL × min, n = 6). Finally, when both groups were euthanized after eight weeks on HFD and tissues harvested for mRNA measurements, both the intrascapular brown adipose tissue (iBAT) and perigonadal adipose tissue (GAT) were dissected and weighed. Both iBAT and GAT mass were significantly less in the *Stim1*^{kko} versus the *Kiss1*^{Cre} females (*Stim1*^{kko} versus the *Kiss1*^{Cre} iBAT: 73.3 ± 6.0 mg, n=10 vs 97.3 ± 9.6 mg, n=10; *Stim1*^{kko} versus the *Kiss1*^{Cre} GAT: 1.5 ± 0.2 g, n=10 vs 2.3 ± 0.2 g, n=10) (***Figures 6F, G***). Overall, these results suggest that conditional deletion of *Stim1* in Kiss1^{ARH} neurons affords some protection against diet-induced obesity. However, we cannot overlook the possible contribution of deletion of *Stim1* in kisspeptin expressing hepatocytes (Song et al., 2014) to this metabolic phenotype.

Stim1^{kko} mice on the C57BL/6 background were viable at the expected Mendelian ratio and did not show any deficits in terms of the onset of female puberty (*i.e.,* vaginal opening). However, since kisspeptin neurons are responsible for the maintenance of the reproductive cycle, and *Stim1* deletion facilitated the synchronous firing of Kiss1^{ARH} neurons, we measured the effects of *Stim1* deletion in Kiss1 neurons on the reproductive cycle. We monitored the estrous cycle of *Stim1*^{kko} and *Kiss1*^{Cre} female mice with vaginal lavage for two weeks before ovariectomy for the metabolic studies. *Stim1*^{kko} female mice exhibited exaggerated estrous cycles versus the *Kiss1*^{Cre} females (***Figure 7B versus 7A***), with significantly more days of estrus versus diestrus (***Figure 7C***). Essentially, over this two week period *Kiss1*^{Cre} females completed three estrous cycles versus only two cycles for the *Stim1*^{kko} females. Although a much more in depth analysis is warranted (*i.e.,* measurement of pulsatile LH), the results are not unexpected based on the prolonged synchronous activity that would be driving LH pulses in these female mice (Clarkson et al., 2017; Qiu J. et al., 2016).

Discussion

For the first time, we show that conditional knockout of *Stim1* significantly reduces store-operated Ca^{2+} entry (SOCE) in Kiss1^{ARH} neurons following thapsigargin-mediated depletion of Ca^{2+} stores. Based on single cell qPCR analysis, *Stim1* mRNA was expressed at approximately two-fold higher levels in Kiss1^{ARH} neurons as compared to *Stim2*, and conditional knockout of *Stim1* did not alter expression of *Stim2* in Kiss1^{ARH} neurons—

i.e., there was no developmental compensation. Selective deletion of *Stim1* in Kiss1^{ARH} neurons augmented the TacR3-mediated increase in $[Ca^{2+}]_i$ and synchronous firing of Kiss1^{ARH} neurons, and this activity was further enhanced by *in vitro* insulin treatment. In addition, whole-cell recording revealed that the slow EPSP induced by high-frequency optogenetic stimulation of Kiss1^{ARH}:ChR2 neurons was also significantly enhanced by *Stim1* deletion. This augmentation of the slow EPSP was mediated by TacR3 coupling to TRPC5 channel activation since the senktide-induced inward current was equally enhanced; and the inward current exhibited the tell-tale double rectifying I/V plot of TRPC5 channels and was antagonized by the TRPC4/5 channel blocker HC070. The rapid insulin effects were abrogated by PI3K kinase inhibitor wortmannin. Importantly, the enhanced TacR3 signaling in *Stim1*^{kko} female mice afforded protection against diet-induced obesity and glucose intolerance.

We first discovered that TRPC5 channels are coupled to metabolic hormone signaling in both POMC and Kiss1^{ARH} neurons (Qiu J. et al., 2011; Qiu J. et al., 2010; Qiu J. et al., 2014). Both leptin and insulin excite/depolarize Kiss1^{ARH} and proopiomelanocortin (POMC) neurons through activation of TRPC5 channels (Kelly Martin J. et al., 2018; Qiu J. et al., 2011; Qiu J. et al., 2010; Qiu J. et al., 2014). In POMC neurons the insulin receptor (InsR) couples to phosphoinositide 3-kinase (PI3K) p110β activation (Al-Qassab et al., 2009; Xu et al., 2005), and the insulin receptor-mediated excitation of POMC and Kiss1^{ARH} neurons is abrogated by inhibition of PI3K activity (Al-Qassab et al., 2009; Hill et al., 2008; Qiu J. et al., 2010; Qiu J. et al., 2014) (**Figure 4**). Activation of PI3K generates PIP_3, which stimulates phospholipase C (PLC) and protein kinase B (Akt) (Bae et al., 1998; Falasca et al., 1998; Qiu J. et al., 2014; Rameh et al., 1998). PLC hydrolyzes PIP_2, which modulates TRPC5 channel activity (Qiu J. et al., 2014; Rodríguez-Menchaca et al., 2012; Zhang, Bosch, et al., 2013). In addition, PI3K quickly increases the vesicular trafficking of TRPC5 channels to the plasma membrane to further boost Ca^{2+} entry into neurons (Bezzerides et al., 2004), which would explain the relatively rapid effects of insulin to increase the slow EPSP following high frequency optogenetic stimulation of Kiss1^{ARH}:ChR2 neurons (**Figure 4**) and the senktide-mediated increase in GCaMP6s activity (**Figure 2**). Therefore, insulin appears to have dual complementary actions to directly activate TRPC5 channels and to mobilize intracellular vesicular pools of TRPC5 channels to augment NKB actions to synchronize Kiss1^{ARH} neuronal firing via PI3K signaling pathways (Qiu J. et al., 2016; Qiu J. et al., 2014).

More recently, we have discovered a critical role of STIM1 in the insulin signaling cascade in POMC neurons (Qiu J., Bosch, et al., 2018). TRPC channels form either receptor-operated cation channels (activated by membrane delimited receptors) or store-operated calcium channels (activated by depletion of calcium stores), which is dependent on their association with STIM1 and plasma membrane calcium channels (*e.g.,* TRPC and Orai channels) to generate SOCE (Birnbaumer, 2009; Salido et al., 2011; Wang H. et al., 2020). Upon depletion of endoplasmic reticulum Ca^{2+}, STIM1 undergoes a conformational change, oligomerizes and then interacts with plasma membrane Orai and TRPC channels to become plasma membrane calcium release-activated calcium (I_{crac}) channels (Huang et al., 2006; Salido et al., 2011; Yuan et al., 2007). *Stim1* mRNA is highly expressed in POMC (Qiu J., Bosch, et al., 2018) and $Kiss1^{ARH}$ neurons (**Figure 1**), and estradiol downregulates *Stim1* mRNA expression, as measured in microdissected arcuate nuclei that encompasses these two populations of neurons. Downregulation of *Stim1* is critical for maintaining insulin excitability in POMC neurons with diet-induced obesity (Qiu J., Bosch, et al., 2018). In ovariectomized females that are relatively refractory to insulin excitation, bath perfusion of a SOCE inhibitor (GSK 7975A) rapidly increases the insulin-mediated excitation of POMC neurons (*i.e*., activation of the TRPC5 mediated inward current), which supports the concept that TRPC5 channels play a role both in SOCE and receptor operated calcium entry (Birnbaumer, 2009; Salido et al., 2011). Therefore, selective deletion of *Stim1* in $Kiss1^{ARH}$ neurons would ensure that TRPC5 channels function as receptor-operated channels to not only couple to insulin (tyrosine kinase) receptors but also to TacR3s to transmit the excitatory effects of NKB to induce synchronous firing of $Kiss1^{ARH}$ neurons as demonstrated in the present findings.

Downregulating STIM1 inhibits SOCE, attenuates Ca^{2+} influx into the ER and elevates intracellular Ca^{2+} levels, which could also contribute to activation of TRPC5 channels in $Kiss1^{ARH}$ neurons (Blair et al., 2009). Indeed, we found that Ca^{2+} greatly potentiated the leptin-induced TRPC5 current in POMC neurons (Qiu J. et al., 2010). In cortical neurons and heterologous cells expressing *Cav1.2* (L-type calcium) channels and *Stim1*, inhibition of STIM1 augments Ca^{2+} influx through L-type calcium channels (Park et al., 2010; Wang Y. et al., 2010). Calcium sensing by STIM1 is also involved in the control of L-type Ca^{2+} channel activity in the hippocampus (Dittmer et al., 2017). In hippocampal pyramidal neurons, glutamate-mediated depolarization

297 activates L-type calcium channels and release of Ca^{2+} from ER stores that activates STIM1, which drives
298 aggregation of the calcium channels to inhibit further L-type channel activity (Dittmer et al., 2017). In
299 cardiomyocyte-derived (HL-1) cells, knocking down STIM1 increases the peak amplitude and current density of
300 T-type calcium channels and shifts the activation curve toward more negative membrane potentials (Nguyen et
301 al., 2013). Furthermore, biotinylation assays reveal that knocking down *Stim1* increases T-type calcium channel
302 surface expression, and co-immunoprecipitation assays suggest that STIM1 directly regulates T-type channel
303 activity (Nguyen et al., 2013). Thus, STIM1 appears to be a negative regulator of T-type channel activity.
304 Moreover, estradiol treatment upregulates *Cav3.1* channel expression by 3-fold and whole cell currents by 10-
305 fold in $Kiss1^{ARH}$ neurons, which greatly enhances the excitability and contributes to synchronous firing of $Kiss1^{ARH}$
306 neurons (Qiu J., Rivera, et al., 2018). The T-type calcium channel Cav3.1 underlies burst firing in rostral
307 hypothalamic kisspeptin neurons (Zhang, Tonsfeldt, et al., 2013) and facilitates TRPC4 channel activation in
308 GnRH neurons (Zhang, Bosch, et al., 2013; Zhang et al., 2008). Cav3.1 channels may also facilitate TRPC5
309 channel opening in $Kiss1^{ARH}$ neurons (**Figure 8**), but this remains to be determined.
310
311 Presumably with conditional knockout, *Stim1* was deleted in all cells expressing kisspeptin, which includes
312 arcuate, anteroventral periventricular preoptic (AVPV) and amygdala kisspeptin neurons, and non-neural
313 kisspeptin cells in the gonads, pancreas and liver (Dudek et al., 2019). Currently, we found that the deletion of
314 *Stim1* in hypothalamic kisspeptin neurons, and possibly the ovarian follicles, disrupted the estrous cycle (**Figure**
315 **7**). Interestingly, $Stim1^{kko}$ mice exhibited more estrous-type vaginal cytology, which is indicative of higher levels
316 of circulating estrogens and maybe the result of increased synchronous firing of kisspeptin neurons and
317 excitatory drive to GnRH neurons (Qiu J. et al., 2016). Because of the well-documented anorexigenic actions
318 of E2 on hypothalamic POMC and AgRP neurons controlling energy homeostasis (Clegg, 2012; Kelly M. J. and
319 Rønnekleiv, 2012; Qiu J. et al., 2006; Roepke et al., 2010; Smith et al., 2013), we ovariectomized the females
320 before feeding them a high fat diet. We tested the hypothesis that *Stim1* deletion in $Kiss1^{ARH}$ neurons would
321 facilitate insulin signaling to maintain energy balance (Navarro Víctor M., 2020; Qiu J., Rivera, et al., 2018). After
322 7 weeks on a high fat diet, $Stim1^{kko}$ females gained modestly less body weight but showed significantly less body
323 fat and lean mass than high fat-dieted, ovariectomized $Kiss1^{Cre}$ females. Most importantly, $Stim1^{kko}$ females

exhibited improved glucose tolerance. Interestingly, the effects of *Stim1* deletion in Kiss1^{ARH} neurons are analogous to the augmented excitatory effects of insulin in POMC neurons following conditional knockout of the T-cell protein tyrosine phosphatase (TCPTP) (Dodd Garron T. et al., 2018). Expression of TCPTP is highly regulated by the metabolic state such that its expression increases in fasted and obese states (Dodd G. T. et al., 2015; Dodd Garron T. et al., 2018). The tyrosine phosphatase through its dephosphorylation of STAT3 inhibits downstream signaling of leptin and insulin in POMC neurons (Dodd Garron T. et al., 2018). Moreover, Kiss1^{ARH} neurons are an integral part of an anorexigenic circuit in the hypothalamus (Navarro Víctor M., 2020; Qiu J., Rivera, et al., 2018; Rønnekleiv et al., 2019) and may provide the excitatory glutamatergic drive to the paraventricular hypothalamus to generate rapid satiety following a meal (Fenselau et al., 2017). However, future experiments will need to test this directly by using ChR2-assisted circuit mapping along with high frequency stimulation of Kiss1^{ARH} neurons to further document this pathway (Qiu J., Rivera, et al., 2018)

Presently, there is compelling evidence that Kiss1^{ARH} neurons are the critical “command” neuron for coordinating energy states with reproductive functions (see (Navarro Víctor M., 2020; Rønnekleiv et al., 2019) for review). Insulin may be the critical metabolic hormone providing feedback since neuron-specific deletion of insulin receptors causes hypothalamic hypogonadism and infertility (Bruning et al., 2000). Moreover, insulin stimulates pulsatile LH secretion by the pituitary gland in diabetic animal models (Bucholtz et al., 2000), and administration of kisspeptin in type 2 diabetic males with central hypogonadism increases LH pulses and enhances gonadal testosterone secretion (George et al., 2013). While it is unclear if GnRH neurons are directly regulated by insulin (Sliwowska et al., 2014), Kiss1^{ARH} neurons express insulin receptors and are robustly depolarized by physiological levels of insulin (Qiu J. et al., 2014; Rønnekleiv et al., 2019). Not only does insulin depolarize Kiss1^{ARH} neurons via opening TRPC5 channels (Qiu J. et al., 2011; Qiu J. et al., 2014), presently we found that insulin increases the excitatory response to NKB to augment synchronous firing of Kiss1^{ARH} neurons. Also, we have now documented that conditional knockout of *Stim1* in Kiss1^{ARH} neurons, which augments the NKB-mediated depolarization of these neurons via TRPC5 channels, helps protect ovariectomized, female mice from diet-induced obesity and glucose intolerance. Therefore, insulin excitation of Kiss1^{ARH} neurons not only enhances synchronous activity (pulse generator activity) to provide excitatory drive to GnRH neurons for

maintaining reproductive functions (Clarkson et al., 2017; Kinsey-Jones et al., 2008; Okamura et al., 2013) but also contributes to energy homeostasis in satiated states (Qiu J., Rivera, et al., 2018; Tolson et al., 2014). Clearly, Kiss1^{ARH} neurons are a CNS center for coordinating reproduction with energy balance, but additional experiments are needed to elucidate the cellular mechanisms by which steroid and metabolic hormonal signaling synergize to govern their activity.

Materials and Methods

Animals

All animal procedures were conducted at Oregon Health and Science University (OHSU) according to the National Institutes of Health Guide for the Care and Use of Laboratory Animals and with approval from the OHSU Animal Care and Use Committee.

We used female mice in all of the experiments. *Kiss1*$^{Cre:GFP}$ (v2) mice (Padilla et al., 2018) were housed under constant temperature (21–23°C) and 12-h light, 12-h dark cycle schedule (lights on at 0600 and lights off at 1800 h), with free access to food (Lab Diets 5L0D) and water. *Kiss1*$^{Cre:GFP}$ mice were used for viral injection to express ChR2 or GCaMP6s in Kiss1^{ARH} neurons or they were crossed with heterozygous *Ai32* mice (RRID:IMSR_JAX:024109, C57BL/6 background) purchased from The Jackson Laboratory. These *Ai32* mice carry the ChR2 (H134R)–EYFP gene in their Gt(ROSA)26Sor locus (Madisen et al., 2012). The gene is separated from its CAG promoter by a loxP-flanked transcriptional STOP cassette, allowing its expression in a Cre-dependent manner. To test for this we dispersed and harvested EYFP neurons in the ARH from *Kiss1*$^{Cre:GFP}$*::Ai32* females and used single cell RT-PCR to determine *Kiss1* mRNA expression as described below and according to previous published methods (Bosch et al., 2013). Data from 158 ARH^{EYFP} neurons from 6 *Kiss1*$^{Cre:GFP}$*::Ai32* females documented that 99% of the EYFP neurons expressed *Kiss1*, which is similar to data obtained from *Kiss1*$^{Cre:GFP}$ females (99% of 448 neurons harvested from 12 females expressed *Kiss1*).

To generate mice with conditional knockout of *Stim1* in Kiss1 neurons (*Stim1*^{kko}), we first crossed *Kiss1*$^{Cre:GFP}$ (v2) mice (Padilla et al., 2018) to *Stim1*$^{lox/lox}$ mice (Jackson Laboratory Stock #023350, RRID:IMSR_JAX:023350, (Oh-hora et al., 2008)). This cross knocks out *Stim1* through excising exon 2 (Oh-hora et al., 2008) of the floxed *Stim1* gene in cells in which Cre is expressed under the control of a promoter specific for the expression of *Kiss1* (Padilla et al., 2018; Qiu J., Rivera, et al., 2018). We then bred *Kiss1*$^{Cre:GFP}$*::Stim1*$^{lox/+}$ males with *Stim1*$^{lox/lox}$ females to get *Kiss1*$^{Cre:GFP}$*::Stim1*$^{lox/lox}$ (*Stim1*^{kko}) mice. To maintain the strain, we bred *Stim1*^{kko} males with *Stim1*$^{lox/lox}$ females. Genotypes for *Stim1* were determined using forward primer JAX#18885 (5'-CGA TGG TCT CAC GGT CTC TA-3') and reverse primer JAX#18886 (5'-GCT CTG CTG ACC TGG AAC TA-3'), which distinguished between lox/lox, lox/+, and +/+ genotypes. Cre genotypes were determined using forward primer 5'-GCG GTC TGG CAG TAA AAA CTA TC3'- and reverse primer 5'-TTC CAT GAG TGA ACG AAC CTG G-3', which distinguished between carriers and non-carriers of the Cre allele.

To determine whether deleting *Stim1* in Kiss1-expressing neurons might impact fertility, we evaluated female *Stim1*^{kko} mice and Cre-negative *Stim1*$^{lox/lox}$ littermates for pubertal onset and estrous cyclicity. Puberty onset in females was assessed by monitoring for vaginal opening daily between 0900 and 1000 hr starting at 3 weeks of age. For estrous cycle studies, female mice were group housed and handled prior to estrous cycle monitoring. Vaginal lavage was performed daily for 4 consecutive weeks between 0900 and 1000 hr. Cytology was evaluated using a light microscope and scored as diestrus, proestrus or estrus as previously described (Qiu J., Rivera, et al., 2018).

Puberty onset and estrous cyclicity

To determine whether deleting *Stim1* in Kiss1-expressing neurons might impact fertility, we evaluated female *Stim1*^{kko} mice and wild type (WT) females littermates for pubertal onset and estrous cyclicity. Puberty onset in females was assessed by monitoring for vaginal opening daily between 0900 and 1000 hr starting at 3 weeks of age. For estrous cycle studies, Kiss1^{kko} and Kiss1$^{Cre:GFP}$ female mice were group housed and were habituated to handling for at least one week by the same investigator prior to estrous cycle monitoring. Vaginal lavage was performed daily for 13 consecutive days between 0900 and 1000 hr. Cytology was evaluated using a light

405 microscope and scored as diestrus, proestrus or estrus as previously described (Qiu J., Rivera, et al., 2018).
406 The Number of estrous and diestrous days were counted for each animal and used for statistical analysis (Mann-
407 Whitney U-test).
408
409 *Gonadectomy*
410
411 When necessary, at least 7 days prior to each experiment, ovaries were removed as described previously
412 while under inhalant isofluorane anesthesia (Piramal Enterprises Limited, Andhra Pradesh, India) {Qiu, 2018,
413 20613}. Each mouse received analgesia (Carprofen; 5mg/kg; subcutaneous) immediately after a surgery for
414 relief of postoperative pain.
415
416 *Metabolic Studies*
417 For the metabolic studies, *Stim1*^{kko} and *Kiss1* littermate control females were ovariectomized at 2-4 months
418 of age and put on a high fat diet (HFD; 45% kcal from fat; Research Diets, New Brunswick, NJ; D12451) for eight
419 weeks. Mice were group housed (because of COVID-19 restrictions) and individually weighed every week. The
420 evening prior to the glucose tolerance test (GTT), all mice were assessed for body composition (fat and lean
421 mass) using an EchoMRI 4-in-1-500 Body Composition Analyzer (Houston, TX).
422
423 For GTT, age matched *Kiss1*^{Cre} and *Stim1*^{kko} mice were fasted for overnight for 15-h, and baseline glucose
424 levels measured with the aid of an Accu-Check Advantage blood glucose meter (Roche) using blood collected
425 from the tail vein. All mice were then injected intraperitoneally with glucose (1 mg/g lean mass as determined by
426 EchoMRI) in sterile PBS and blood glucose levels were measured 15, 30, 60, 90, and 120 min after injection.
427 The glucose clearance (area under the curve) was calculated based on the glucose baseline levels at 0 min
428 (Ayala et al., 2010).
429
430
431 *AAV delivery to Kiss1*$^{Cre:GFP}$ *and Stim1*^{kko} *mice*

Fourteen to twenty-one days prior to each experiment, *Kiss1*$^{Cre:GFP}$ mice or *Stim1*^{kko} mice (>60 days old) received bilateral ARH injections of a Cre-dependent adeno-associated viral (AAV; serotype 1) vector encoding ChR2-mCherry (AAV1-Ef1a-DIO-ChR2: mCherry) or ChR2-YFP (AAV1-Ef1a-DIO-ChR2:YFP) or GCaMP6s (AAV9-Syn-Flex-GCaMP6s-WPRE-SV40). Using aseptic techniques, anesthetized female mice (1.5% isoflurane/O_2) received a medial skin incision to expose the surface of the skull. The glass pipette (Drummond Scientific #3-000-203-G/X; Broomall, PA) with a beveled tip (diameter = 45 mm) was filled with mineral oil, loaded with an aliquot of AAV using a Nanoject II (Drummond Scientific). ARH injection coordinates were anteroposterior (AP): −1.20 mm, mediolateral (ML): ± 0.30 mm, dorsoventral (DL): −5.80 mm (surface of brain z = 0.0 mm); 500 nl of the AAV (2.0 x 10^{12} particles/ml) was injected (100 nl/min) into each position, left in place for 10 min post-injection, then the pipette was slowly removed from the brain. The skin incision was closed using skin adhesive, and each mouse received analgesia (Carprofenl; 5 mg/kg) for two days post-operation.

Electrophysiology

Coronal brain slices (250 μm) containing the ARH from gonadectomized females were prepared as previously described (Qiu J. et al., 2003). Whole-cell, patch recordings were performed in voltage clamp and current clamp using an Olympus BX51W1 upright microscope equipped with video-enhanced, infrared-differential interference contrast (IR-DIC) and an Exfo X-Cite 120 Series fluorescence light source. Electrodes were fabricated from borosilicate glass (1.5 mm outer diameter; World Precision Instruments, Sarasota, FL) and filled with a normal internal solution (in mM): 128 potassium gluconate, 10 NaCl, 1 $MgCl_2$, 11 EGTA, 10 HEPES, 3 ATP, and 0.25 GTP (pH was adjusted to 7.3–7.4 with 1N KOH, 290–300 mOsm). Pipette resistances ranged from 3–5 MΩ. In whole cell configuration, access resistance was less than 20 MΩ; access resistance was 80% compensated. For optogenetic stimulation, a light-induced response was evoked using a light-emitting diode (LED) 470 nm blue light source controlled by a variable 2A driver (ThorLabs, Newton, NJ) with the light path delivered directly through an Olympus 40 water-immersion lens. High fidelity response to light (470 nm) stimulation of Kiss1^{ARH} ::ChR2-mCherry expressing neurons was observed, and both evoked inward currents (in

voltage clamp, V_{hold} = −60 mV) or depolarization (in current clamp) were measured. Electrophysiological signals were amplified with an Axopatch 200A and digitized with Digidata 1322A (Molecular Devices, Foster City, CA), and the data were analyzed using p-Clamp software (RRID:SCR_011323, version 9.2, Molecular Devices). The amplitude of the slow EPSP was measured after low pass filtering in order to eliminate the barrage of action potentials riding on the depolarization. The liquid junction potential was corrected for all data analysis.

Calcium imaging

For calcium imaging, brain slices were placed in a RC-22C slide recording chamber (Harvard/Warner Instruments) and imaged on an inverted Nikon TiE microscope equipped with a Yokogawa CSU-W1 spinning disk confocal head, integrated under NIS Elements v4.20 (Nikon). The preparation, kept at 32°C via a cage incubator (Okolab), was continuously perfused with oxygenated aCSF at a flow rate of 1.25 ml/min. Images were acquired on a Zyla v5.5 sCMOS camera (Andor) at 0.5 Hz. frame-rate, through an 10 x (NA 0.45) or 20 x (NA 0.75) objective, combining 488 nm laser excitation with 500–550 nm emission collection. Changes in $Kiss1^{ARH}$ neuron Ca^{2+} levels were measured in regions of interest (ROIs) comprising the GCaMP6s-positive cell bodies. In all recordings, background fluorescence measured in an ROI drawn on nearby tissue was subtracted from every ROI. $[Ca^{2+}]_i$ variations after drug applications were assessed as changes in fluorescence signals over baseline ($\Delta F/F_0$). To normalize the fluorescence value of each cell, we first separated experimental trials into two parts: a baseline period (2 min) corresponding to all the frames recorded before addition of drugs, and a stimulus period, after the onset of the drug (such as bath-applied senktide) application and lasting several minutes. Next, for each ROI we calculated $\Delta F/F_0$ for each frame (t), where $\Delta F/F_0$ equals $(F_{(t)} - F_0)/F_0$, and F_0 was the mean fluorescence value for that ROI for all frames in the baseline period for that trial. The area under the curve (AUC) was calculated over the time period of 2 min before and the 18 min after drug application. Maximal peak reached after drug application was also measured and used in quantitative analysis. Data were averaged across all $Kiss1^{ARH}$ neurons in a slice (two slices per animal), which were used as the statistical unit over a minimum of 3 animals per condition.

Single cell RT-PCR (scRT-PCR)

Coronal brain sections from the ARH of three female *Stim1*^{kko} and three *Kiss1*$^{Cre:GFP}$*::Ai32* mice were prepared for electrophysiology. The 3-4 sections obtained were divided between electrophysiological recording experiments and single cell harvesting. Single cell dispersion and harvesting was performed as described previously with some modifcations (Bosch et al., 2013; Zhang, Tonsfeldt, et al., 2013). Briefly, the ARH was dissected and digested in papain (Sigma). Gentle trituration using varying sizes of flame polished Pasteur pipets were used to disperse the cells and then they were plated onto a glass bottom dish. A constant flow of oxygenated aCSF (NaCl, 125 mM; KCl, 5 mM; NaH_2PO_4, 1.44 mM; Hepes, 5 mM; D-glucose, 10 mM; $NaHCO_3$, 26 mM; $MgSO_4{\cdot}7H_2O$, 2 mM; $CaCl_2$, 2 mM) was applied to the dish to keep the cells healthy and to clear debris. Fluorescent neurons were visualized under an inverted microscope. The Xenoworks Microinjection system (Sutter Instruments) was used to manipulate a 10 µm tip size glass capillary tube to approach single neurons, apply gently suction and harvest single cells or pools of 10 cells into a siliconized tube containing a solution of 1X Invitrogen Superscript III Buffer (LifeTech), 15U of RNasin (Promega), 10 mM of dithiothreitol (DTT) and diethylpyrocarbonate (DEPC)-treated water in a total of 5 µl for single cells or 8 µl for pools of 10 cells. Corresponding controls were collected at the same time including single neurons (processed without reverse transcriptase) and aCSF from the surrounding area. Hypothalamic tissue RNA was also processed with and without reverse transcriptase. First strand cDNA synthesis was performed on single cells, pools of cells and controls in a 20 µl (single cells) or 25 µl (10 cell pools) volume containing a final concentration of 1X Invitrogen Superscript III Buffer, 30 U of RNasin, 15 mM DTT, 10 mM dNTP, 100 ng Random Primers (Promega), 400 ng Anchored Oligo $(dT)_{20}$ Primer (Invitrogen), 100 U Superscript III Reverse Transcriptase (Life Tech) and DEPC-treated water according to manufactures protocol and stored at -20°C. Clone Manager software (Sci Ed Software) was used to design primers that cross at least one intron-exon boundary. In order to confirm that STIM1 was knocked out, STIM1 primers were designed to include part of exon 2 (see Table 1). Single cell PCR conditions were optimized for primer concentration, magnesium concentration and annealing temperature. Standard curves were generated using hypothalamic cDNA with dilutions from 1:50 to 1:12,800 for primers used for qPCR to determine the efficiency ($E = 10^{(-1/m)}$-1; table 1). Primer pairs with efficiencies of 90-100% permit

the use of the comparative ΔΔCT method for analysis (Livak and Schmittgen, 2001; Pfaffl, 2001).

PCR was performed on 3 µl of cDNA from single cells in a 30 µl reaction volume containing 1X GoTaq Flexi buffer (Promega), 2 mM $MgCl_2$, 10 mM dNTP, 0.33 µM forward and reverse primers, 2 U GoTaq Flexi Polymerase (Promega) and 0.22 µg TaqStart Antibody (Clontech). 45-50 cycles of amplification were performed on a Bio-Rad C1000 thermocycler and the resulting product visualized with ethidium bromide on a 2% agarose gel.

Quantitative PCR was performed on 4 µl of cDNA from pools of 10 cells (4 pools/animal) in duplicate for the target genes (*Stim1*, *Stim2*) and 2 µl in duplicate for the reference gene (*Gapdh*) in a 20 µl reaction volume containing 1X Power SYBR Green PCR Master Mix (Applied Biosystems) and 0.5 µM forward and reverse primers. Forty cycles of amplification were run on a Quant Studio 7 Flex Real-Time PCR System (Applied Biosystems) and the resulting data was analyzed using the comparative ΔΔCT method (Livak and Schmittgen, 2001; Pfaffl, 2001). The relative linear quantity was determined with the $2^{-\Delta\Delta CT}$ equation (Bosch et al., 2013). The mean of all of the ΔCT values (ΔCT = CT of the target gene – CT of the reference gene) from the controls was used as the calibrator and the data is expressed as fold change in gene expression.

Drugs

A standard artificial cerebrospinal fluid was used (Qiu J. et al., 2011). All drugs were purchased from Tocris Bioscience (Minneapolis, MN) unless otherwise specified. Purified guinea pig insulin was purchased from Dr. Al Parlow (Harbor-UCLA Medical Center, Torrance, CA, USA) through the National Hormone and Peptide Program. Tetrodotoxin (TTX) was purchased from Alomone Labs (Jerusalem, Israel) (1 mM) and dissolved in H_2O. Thapsigargin (Tg, 2 mM), TacR3 agonist senktide (1 mM), TRPC4/5 antagonist, HC 070 (from MCE, 10 mM), and the PI3K inhibitor wortmannin (Alomone Labs; 100 µM) were prepared in dimethylsulfoxide (DMSO). Aliquots of the stock solutions were stored as appropriate until needed.

Data analysis

For qPCR four Kiss1 neuronal pools (10 cells/pool) from each animal were run in duplicate for the mRNAs that encode for STIM1, STIM2 and GAPDH and the mean value of each gene from each animal was used for statistical analysis. Data are expressed as Mean ± SEM and were analyzed using an unpaired student's t-test. For scRT-PCR the number of Kiss1-positive cells harvested from $Kiss1^{Cre:GFP}$ females injected with Cre-dependent ChR2-mCherry or from $Kiss1^{Cre:GFP}$::Ai32 females were determined. Subsequently, the Kiss1-positive cells also positive for STIM1 and STIM2 were counted and used to qualitatively assess the number of Kiss1 neurons with Stim1 and Stim2 and percent expression.

Comparisons between different treatments were performed using a repeated measures, two-way or one-way ANOVA analysis with the *post hoc* Bonferroni's test. Differences were considered statistically significant if $p < 0.05$. All data are expressed as mean ± SEM.

Acknowledgements

We thank Mr. Daniel Johnson for his technical support.

Statement of Ethics

Animal experimentation: This study was performed in strict accordance with the recommendations from the National Institutes of Health Guide for the care and use of Laboratory Animals. All animal procedures were conducted according to the approved institutional animal care and use committee (IACUC) protocols (#IP00000585; #IP00000382) at Oregon health and Science University. All surgeries were performed using aseptic techniques under isoflurane anesthesia, and every effort was made to minimize pain and suffering.

Disclosure Statement

The authors declare that no competing interests exist.

Funding Sources

This research was funded by National Institute of Health (NIH) grants: R01-NS043330 (OKR), R01-NS038809 (MJK) and R01-DK068098 (OKR and MJK). Confocal microscopy was supported by a P30 NS061800 (PI, S Aicher) grant.

Author Contributions

Jian Qiu, Todd L Stincic, Martha A Bosch, Ashley Connors, Data curation, Methodology, Writing—review and editing; Stefanie Kaech Petrie, Resources, Methodology, Writing—review and editing; Oline K Rønnekleiv, Martin J Kelly, Conceptualization, Resources, Data curation, Supervision, Funding acquisition, Validation, Methodology, Project administration, Writing—review and editing.

References

Al-Qassab H, Smith MA, Irvine EE, Guillermet-Guibert J, Claret M, Choudhury AI, Selman C, Piipari K, Clements M, Lingard S, Chandarana K, Bell JD, Barsh GS, Smith AJH, Batterham RL, Ashford MLJ, Vanhaesebroeck B, & Withers DJ. 2009. Dominant role of the p110β isoform of PI3K over p110α in energy homeostasis regulation by POMC and AgRP neurons. *Cell Metabolism* **10**: 343-354. DOI:10.1016/j.cmet.2009.09.008, PMID: 19883613.

Aponte Y, Atasoy D, & Sternson SM. 2011. AGRP neurons are sufficient to orchestrate feeding behavior rapidly and without training. *Nature Neuroscience* **14**: 351-355. DOI:10.1038/nn.2739, PMID: 21209617.

Ayala JE, Samuel VT, Morton GJ, Obici S, Croniger CM, Shulman GI, Wasserman DH, McGuinness OP, & Consortium NIHMMPC. 2010. Standard operating procedures for describing and performing metabolic tests of glucose homeostasis in mice. *Disease Models & Mechanisms* **3**: 525-534. DOI:10.1242/dmm.006239, PMID: 20713647.

Bae YS, Cantley LG, Chen C-S, Kim S-R, Kwon K-S, & Rhee SG. 1998. Activation of phospholipase C-γ by phosphatidylinositol 3,4,5-trisphosphate. *Journal of Biological Chemistry* **273**: 4465-4469.

DOI:10.1074/jbc.273.8.4465, PMID: 9468499.

Benoit SC, Air EL, Coolen LM, Strauss R, Jackman A, Clegg DJ, Seeley RJ, & Woods SC. 2002. The catabolic action of insulin in the brain is mediated by melanocortins. *The Journal of Neuroscience* **22**: 9048-9052. DOI:10.1523/JNEUROSCI.22-20-09048.2002, PMID: 12388611.

Berna-Erro A, Braun A, Kraft R, Kleinschnitz C, Schuhmann MK, Stegner D, Wultsch T, Eilers J, Meuth SG, Stoll G, & Nieswandt B. 2009. STIM2 Regulates Capacitive Ca^{2+} Entry in Neurons and Plays a Key Role in Hypoxic Neuronal Cell Death. *Science Signaling* **2**: ra67-ra67. DOI:10.1126/scisignal.2000522, PMID: 19843959.

Bezzerides VJ, Ramsey IS, Kotecha S, Greka A, & Clapham DE. 2004. Rapid vesicular translocation and insertion of TRP channels. *Nature Cell Biology* **6**: 709-720. DOI:10.1038/ncb1150, PMID: 15258588.

Birnbaumer L. 2009. The TRPC class of ion channels: a critical review of their roles in slow, sustained increases in intracellular Ca^{2+} concentrations. *Annual Review of Pharmacology and Toxicology* **49**: 395-426. DOI:10.1146/annurev.pharmtox.48.113006.094928, PMID: 19281310.

Blair NT, Kaczmarek JS, & Clapham DE. 2009. Intracellular calcium strongly potentiates agonist-activated TRPC5 channels. *The Journal of General Physiology* **133**: 525-546. DOI:10.1085/jgp.200810153, PMID: 19398778.

Bosch MA, Tonsfeldt KJ, & Rønnekleiv OK. 2013. mRNA expression of ion channels in GnRH neurons: subtype-specific regulation by 17β-Estradiol. *Molecular and Cellular Endocrinology* **367**: 85-97. DOI:10.1016/j.mce.2012.12.021, PMID: 23305677.

Brini M, Calì T, Ottolini D, & Carafoli E. 2014. Neuronal calcium signaling: function and dysfunction. *Cellular and Molecular Life Sciences* **71**: 2787-2814. DOI:10.1007/s00018-013-1550-7, PMID: 24442513.

Brown LM, Clegg DJ, Benoit SC, & Woods SC. 2006. Intraventricular insulin and leptin reduce food intake and body weight in C57BL/6J mice. *Physiology & Behavior* **89**: 687-691. DOI:10.1016/j.physbeh.2006.08.008, PMID: 16979194.

Bruning JC, Gautam D, Burks DJ, Gillette J, Schubert M, Orban PC, Klein R, Krone W, Muller-Wieland D, & Kahn CR. 2000. Role of brain insulin receptor in control of body weight and reproduction. *Science* **289**: 2122-2125. DOI:10.1126/science.289.5487.2122, PMID: 11000114.

621 Bucholtz DC, Chiesa A, Pappano WN, Nagatani S, Tsukamura H, Maeda K-I, & Foster DL. 2000. Regulation of
622 Pulsatile Luteinizing Hormone Secretion by Insulin in the Diabetic Male Lamb1. *Biology of Reproduction*
623 **62**: 1248-1255. DOI:10.1095/biolreprod62.5.1248, PMID: 10775173.
624 Clarkson J, Han SY, Piet R, McLennan T, Kane GM, Ng J, Porteous RW, Kim JS, Colledge WH, Iremonger KJ,
625 & Herbison AE. 2017. Definition of the hypothalamic GnRH pulse generator in mice. *Proceedings of the*
626 *National Academy of Sciences of the United States of America* **114**: E10216-E10223.
627 DOI:10.1073/pnas.1713897114, PMID: 29109258.
628 Clegg DJ. 2012. Minireview: the year in review of estrogen regulation of metabolism. *Molecular Endocrinology*
629 **26**: 1957-1960. DOI:10.1210/me.2012-1284, PMID: 23051593.
630 Clegg DJ, Gotoh K, Kemp C, Wortman MD, Benoit SC, Brown LM, D'Alessio D, Tso P, Seeley RJ, & Woods
631 SC. 2011. Consumption of a high-fat diet induces central insulin resistance independent of adiposity.
632 *Physiology & Behavior* **103**: 10-16. DOI:10.1016/j.physbeh.2011.01.010, PMID: 21241723.
633 de Croft S, Boehm U, & Herbison AE. 2013. Neurokinin B activates arcuate kisspeptin neurons through
634 multiple tachykinin receptors in the male mouse. *Endocrinology* **154**: 2750-2760. DOI:10.1210/en.2013-
635 1231, PMID: 23744641.
636 Dittmer PJ, Wild AR, Dell'Acqua ML, & Sather WA. 2017. STIM1 Ca^{2+} Sensor Control of L-type Ca^{2+}-Channel-
637 Dependent Dendritic Spine Structural Plasticity and Nuclear Signaling. *Cell Reports* **19**: 321-334.
638 DOI:10.1016/j.celrep.2017.03.056, PMID: 28402855.
639 Dodd GT, Decherf S, Loh K, Simonds SE, Wiede F, Balland E, Merry TL, Munzberg H, Zhang ZY, Kahn BB,
640 Neel BG, Bence KK, Andrews ZB, Cowley MA, & Tiganis T. 2015. Leptin and insulin act on POMC
641 neurons to promote the browning of white fat. *Cell* **160**: 88-104. DOI:10.1016/j.cell.2014.12.022, PMID:
642 25594176.
643 Dodd GT, Michael NJ, Lee-Young RS, Mangiafico SP, Pryor JT, Munder AC, Simonds SE, Brüning JC, Zhang
644 Z-Y, Cowley MA, Andrikopoulos S, Horvath TL, Spanswick D, & Tiganis T. 2018. Insulin regulates
645 POMC neuronal plasticity to control glucose metabolism. *eLife* **7**: e38704. DOI:10.7554/eLife.38704,
646 Dudek M, Ziarniak K, Cateau M-L, Dufourny L, & Sliwowska JH. 2019. Diabetes type 2 and kisspeptin: Central
647 and peripheral sex-specific actions. *Trends in Endocrinology & Metabolism* **30**: 833-843.

DOI:https://doi.org/10.1016/j.tem.2019.07.002,

Falasca M, Logan SK, Lehto VP, Baccante G, Lemmon MA, & Schlessinger J. 1998. Activation of phospholipase Cγ by PI 3-kinase-induced PH domain-mediated membrane targeting. *The EMBO Journal* **17**: 414-422. DOI:10.1093/emboj/17.2.414, PMID: 9430633.

Fenselau H, Campbell JN, Verstegen AM, Madara JC, Xu J, Shah BP, Resch JM, Yang Z, Mandelblat-Cerf Y, Livneh Y, & Lowell BB. 2017. A rapidly acting glutamatergic ARC→PVH satiety circuit postsynaptically regulated by α-MSH. *Nature Neuroscience* **20**: 42-51. DOI:10.1038/nn.4442, PMID: 27869800.

Gao Y, Yao T, Deng Z, Sohn J-W, Sun J, Huang Y, Kong X, Yu K-J, Wang R-T, Chen H, Guo H, Yan J, Cunningham KA, Chang Y, Liu T, & Williams KW. 2017. TrpC5 mediates acute leptin and serotonin effects via *Pomc* neurons. *Cell Reports* **18**: 583-592. DOI:10.1016/j.celrep.2016.12.072, PMID: 28099839.

George JT, Veldhuis JD, Tena-Sempere M, Millar RP, & Anderson RA. 2013. Exploring the pathophysiology of hypogonadism in men with type 2 diabetes: kisspeptin-10 stimulates serum testosterone and LH secretion in men with type 2 diabetes and mild biochemical hypogonadism. *Clin Endocrinol (Oxf)* **79**: 100-104. DOI:10.1111/cen.12103, PMID: 23153270.

Goodman RL, Lehman MN, Smith JT, Coolen LM, de Oliveira CVR, Jafarzadehshirazi MR, Pereira A, Iqbal J, Caraty A, Ciofi P, & Clarke IJ. 2007. Kisspeptin neurons in the arcuate nucleus of the ewe express both dynorphin A and neurokinin B. *Endocrinology* **148**: 5752-5760. DOI:10.1210/en.2007-0961, PMID: 17823266.

Gruszczynska-Biegala J, Pomorski P, Wisniewska MB, & Kuznicki J. 2011. Differential Roles for STIM1 and STIM2 in Store-Operated Calcium Entry in Rat Neurons. *PLOS One* **6**: e19285. DOI:10.1371/journal.pone.0019285, PMID: 21541286.

Guner G, Guzelsoy G, Isleyen FS, Sahin GS, Akkaya C, Bayam E, Kotan EI, Kabakcioglu A, & Ince-Dunn G. 2017. NEUROD2 Regulates *Stim1* Expression and Store-Operated Calcium Entry in Cortical Neurons. *eNeuro* **4**: ENEURO.0255-0216.2017. DOI:10.1523/eneuro.0255-16.2017, PMID: 28303257.

Hartmann J, Karl RM, Alexander RP, Adelsberger H, Brill MS, Rühlmann C, Ansel A, Sakimura K, Baba Y, Kurosaki T, Misgeld T, & Konnerth A. 2014. STIM1 controls neuronal Ca^{2+} signaling, mGluR1-

675 dependent synaptic transmission, and cerebellar motor behavior. *Neuron* **82**: 635-644.
676 DOI:10.1016/j.neuron.2014.03.027, PMID: 24811382.

677 Hill JW, Williams KW, Ye C, Luo J, Balthasar N, Coppari R, Cowley MA, Cantley LC, Lowell BB, & Elmquist JK.
678 2008. Acute effects of leptin require PI3K signalng in hypothalamic proopiomelanocortin neurons in
679 mice. *Journal of Clinical Investigation* **118**: 1796-1805. DOI:10.1172/JCI32964, PMID: 18382766.

680 Huang GN, Zeng W, Kim JY, Yuan JP, Han L, Muallem S, & Worley PF. 2006. STIM1 carboxyl-terminus
681 activates native SOC, I_{crac} and TRPC1 channels. *Nature Cell Biology* **8**: 1003-1010.
682 DOI:10.1038/ncb1454, PMID: 16906149.

683 Just S, Chenard BL, Ceci A, Strassmaier T, Chong JA, Blair NT, Gallaschun RJ, del Camino D, Cantin S,
684 D'Amours M, Eickmeier C, Fanger CM, Hecker C, Hessler DP, Hengerer B, Kroker KS, Malekiani S,
685 Mihalek R, McLaughlin J, Rast G, Witek J, Sauer A, Pryce CR, & Moran MM. 2018. Treatment with HC-
686 070, a potent inhibitor of TRPC4 and TRPC5, leads to anxiolytic and antidepressant effects in mice.
687 *PLOS One* **13**: e0191225. DOI:10.1371/journal.pone.0191225, PMID: 29385160.

688 Kelly MJ, Qiu J, & Rønnekleiv OK. 2018. TRPCing around the hypothalamus. *Frontiers in Neuroendocrinology*
689 **51**: 116-124. DOI:10.1016/j.yfrne.2018.05.004, PMID: 29859883.

690 Kelly MJ, & Rønnekleiv OK. 2012. Membrane-initiated actions of estradiol that regulate reproduction, energy
691 balance and body temperature. *Frontiers in Neuroendocrinology* **33**: 376-387.

692 Kim D, Jang S, Kim J, Park I, Ku K, Choi M, Lee S, Heo WD, Son GH, Choe HK, & Kim K. 2020. Kisspeptin
693 Neuron-Specific and Self-Sustained Calcium Oscillation in the Hypothalamic Arcuate Nucleus of
694 Neonatal Mice: Regulatory Factors of its Synchronization. *Neuroendocrinology*.
695 DOI:10.1159/000505922, PMID: 31935735.

696 Kinsey-Jones JS, Li XF, Luckman SM, & O'Byrne KT. 2008. Effects of kisspeptin-10 on the
697 electrophysiological manifestation of gonadotropin-releasing hormone pulse generator activity in the
698 female rat. *Endocrinology* **149**: 1004-1008. DOI:10.1210/en.2007-1505, PMID: 18063679.

699 Knobil E. 1981. Patterns of hypophysiotropic signals and gonadotropin secretion in the rhesus monkey. *Biology*
700 *of Reproduction* **24**: 44-49. DOI:10.1095/biolreprod24.1.44, PMID: 6781549.

701 Krashes MJ, Koda S, Ye C, Rogan SC, Adams AC, Cusher DS, Maratos-Flier E, Roth BL, & Lowell BB. 2011.

Rapid, reversible activation of AgRP neurons drives feeding behavior in mice. *Journal of Clinical Investigation* **121**: 1424-1428. DOI:10.1172/JCI46229, PMID: 21364278.

Lehman MN, Coolen LM, & Goodman RL. 2010. Minireview: kisspeptin/neurokinin B/dynorphin (KNDy) cells of the arcuate nucleus: a central node in the control of gonadotropin-releasing hormone secretion. *Endocrinology* **151**: 3479-3489. DOI:10.1210/en.2010-0022, PMID: 20501670.

Livak KJ, & Schmittgen TD. 2001. Analysis of relative gene expression data using real-time quantitative PCR and the $2^{-\Delta\Delta CT}$ method. *Methods* **25**: 402-408. DOI:10.1006/meth.2001.1262, PMID: 11846609.

Madisen L, Mao T, Koch H, Zhuo JM, Berenyi A, Fujisawa S, Hsu YW, Garcia AJ, 3rd, Gu X, Zanella S, Kidney J, Gu H, Mao Y, Hooks BM, Boyden ES, Buzsaki G, Ramirez JM, Jones AR, Svoboda K, Han X, Turner EE, & Zeng H. 2012. A toolbox of Cre-dependent optogenetic transgenic mice for light-induced activation and silencing. *Nature Neuroscience* **15**: 793-802. DOI:10.1038/nn.3078, PMID: 22446880.

Moccia F, Zuccolo E, Soda T, Tanzi F, Guerra G, Mapelli L, Lodola F, & D'Angelo E. 2015. Stim and Orai proteins in neuronal Ca^{2+} signaling and excitability. *Frontiers in Cellular Neuroscience* **9**: 153. DOI:10.3389/fncel.2015.00153, PMID: 25964739.

Navarro VM. 2020. Metabolic regulation of kisspeptin — the link between energy balance and reproduction. *Nature Reviews Endocrinology*. DOI:10.1038/s41574-020-0363-7, PMID: 32427949.

Navarro VM, Castellano JM, McConkey SM, Pineda R, Ruiz-Pino F, Pinilla L, Clifton DK, Tena-Sempere M, & Steiner RA. 2011. Interactions between kisspeptin and neurokinin B in the control of GnRH secretion in the female rat. *American Journal of Physiology: Endocrinology and Metabolism* **300**: E202-E210. DOI:10.1152/ajpendo.00517.2010, PMID: 21045176.

Navarro VM, Gottsch ML, Chavkin C, Okamura H, Clifton DK, & Steiner RA. 2009. Regulation of gonadotropin-releasing hormone secretion by kisspeptin/dynorphin/neurokinin B neurons in the arcuate nucleus of the mouse. *The Journal of Neuroscience* **29**: 11859-11866. DOI:10.1523/JNEUROSCI.1569-09.2009, PMID: 19776272.

Nguyen N, Biet M, Simard É, Bèliveau É, Francoeur N, Guillemette G, Dumaine R, Grandbois M, & Boulay G. 2013. STIM1 participates in the contractile rhythmicity of HL-1 cells by moderating T-type Ca^{2+} channel activity. *Biochimica et Biophysica Acta* **1833**: 1294-1303. DOI:10.1016/j.bbamcr.2013.02.027, PMID:

23458835.

Oh-hora M, Yamashita M, Hogan PG, Sharma S, Lamperti E, Chung W, Prakriya M, Feske S, & Rao A. 2008. Dual functions for the endoplasmic reticulum calcium sensors STIM1 and STIM2 in T cell activation and tolerance. *Nature Immunology* **9**: 432-443. DOI:10.1038/ni1574, PMID: 18327260.

Okamura H, Tsukamura H, Ohkura S, Uenoyama Y, Wakabayashi Y, & Maeda K. 2013. Kisspeptin and GnRH pulse generation. *Advances in Experimental Medicine and Biology* **784**: 297-323. DOI:10.1007/978-1-4614-6199-9_14, PMID: 23550012.

Padilla SL, Johnson CW, Barker FD, Patterson MA, & Palmiter RD. 2018. A neural circuit underlying the generation of hot flushes. *Cell Reports* **24**: 271-277. DOI:10.1016/j.celrep.2018.06.037, PMID: 29996088.

Padilla SL, Perez JG, Ben-Hamo M, Johnson CW, Sanchez REA, Bussi IL, Palmiter RD, & de la Iglesia HO. 2019. Kisspeptin neurons in the arcuate nucleus of the hypothalamus orchestrate circadian rhythms and metabolism. *Current Biology* **29**: 592-604 e594. DOI:10.1016/j.cub.2019.01.022, PMID: 30744968.

Park CY, Shcheglovitov A, & Dolmetsch R. 2010. The CRAC channel activator STIM1 binds and inhibits L-type voltage-gated calcium channels. *Science* **330**: 101-105. DOI:10.1126/science.1191027, PMID: 20929812.

Pavez M, Thompson AC, Arnott HJ, Mitchell CB, D'Atri I, Don EK, Chilton JK, Scott EK, Lin JY, Young KM, Gasperini RJ, & Foa L. 2019. STIM1 Is Required for Remodeling of the Endoplasmic Reticulum and Microtubule Cytoskeleton in Steering Growth Cones. *The Journal of Neuroscience* **39**: 5095-5114. DOI:10.1523/jneurosci.2496-18.2019, PMID: 31023836.

Pfaffl MW. 2001. A new mathematical model for relative quantification in real-time RT-PCR. *Nucleic Acids Research* **29**: e45. DOI:10.1093/nar/29.9.e45, PMID: 11328886.

Qiu J, Bosch MA, Meza C, Navarro UV, Nestor CC, Wagner EJ, Rønnekleiv OK, & Kelly MJ. 2018. Estradiol protects proopiomelanocortin neurons against insulin resistance. *Endocrinology* **159**: 647-664. DOI:10.1210/en.2017-00793, PMID: 29165691.

Qiu J, Bosch MA, Tobias SC, Grandy DK, Scanlan TS, Rønnekleiv OK, & Kelly MJ. 2003. Rapid signaling of estrogen in hypothalamic neurons involves a novel G-protein-coupled estrogen receptor that activates

protein kinase C. *The Journal of Neuroscience* **23**: 9529-9540. DOI:10.1523/JNEUROSCI.23-29-09529.2003, PMID: 14573532.

Qiu J, Bosch MA, Tobias SC, Krust A, Graham S, Murphy S, Korach KS, Chambon P, Scanlan TS, Rønnekleiv OK, & Kelly MJ. 2006. A G-protein-coupled estrogen receptor is involved in hypothalamic control of energy homeostasis. *The Journal of Neuroscience* **26**: 5649-5655. DOI:10.1523/JNEUROSCI.0327-06.2006, PMID: 16723521.

Qiu J, Bosch MA, Zhang C, Rønnekleiv OK, & Kelly MJ. 2020. Estradiol protects neuropeptide Y/agouti-related peptide neurons against insulin resistance in females. *Neuroendocrinology* **110**: 105-118. DOI:10.1159/000501560, PMID: 31212279.

Qiu J, Fang Y, Bosch MA, Rønnekleiv OK, & Kelly MJ. 2011. Guinea pig kisspeptin neurons are depolarized by leptin via activation of TRPC channels. *Endocrinology* **152**: 1503-1514. DOI:10.1210/en.2010-1285, PMID: 21285322.

Qiu J, Fang Y, Rønnekleiv OK, & Kelly MJ. 2010. Leptin excites proopiomelanocortin neurons via activation of TRPC channels. *The Journal of Neuroscience* **30**: 1560-1565. DOI:10.1523/JNEUROSCI.4816-09.2010, PMID: 20107083.

Qiu J, Nestor CC, Zhang C, Padilla SL, Palmiter RD, Kelly MJ, & Rønnekleiv OK. 2016. High-frequency stimulation-induced peptide release synchronizes arcuate kisspeptin neurons and excited GnRH neurons. *eLife* **5**: e16246. DOI:10.7554/eLife.16246, PMID: 27549338.

Qiu J, Rivera HM, Bosch MA, Padilla SL, Stincic TL, Palmiter RD, Kelly MJ, & Rønnekleiv OK. 2018. Estrogenic-dependent glutamatergic neurotransmission from kisspeptin neurons governs feeding circuits in females. *eLife* **7**: e35656. DOI:10.7554/eLife.35656, PMID: 30079889.

Qiu J, Wagner EJ, Rønnekleiv OK, & Kelly MJ. 2018. Insulin and leptin excite anorexigenic pro-opiomelanocortin neurones via activation of TRPC5 channels. *Journal of Neuroendocrinology* **30**: e12501. DOI:10.1111/jne.12501, PMID: 28675783.

Qiu J, Zhang C, Borgquist A, Nestor CC, Smith AW, Bosch MA, Ku S, Wagner EJ, Rønnekleiv OK, & Kelly MJ. 2014. Insulin excites anorexigenic proopiomelanocortin neurons via activation of canonical transient receptor potential channels. *Cell Metabolism* **19**: 682-693. DOI:10.1016/j.cmet.2014.03.004, PMID:

24703699.

Qiu X, Dowling AR, Marino JS, Faulkner LD, Bryant B, Bruning JC, Elias CF, & Hill JW. 2013. Delayed puberty but normal fertility in mice with selective deletion of insulin receptors from Kiss1 cells. *Endocrinology* **154**: 1337-1348. DOI:10.1210/en.2012-2056, PMID: 23392256.

Rameh LE, Rhee SG, Spokes K, Kazlauskas A, Cantley LC, & Cantley LG. 1998. Phosphoinositide 3-kinase regulates phospholipase Cγ-mediated calcium signaling. *Journal of Biological Chemistry* **273**: 23750-23757. DOI:10.1074/jbc.273.37.23750, PMID: 9726983.

Rodríguez-Menchaca AA, Adney SK, Zhou L, & Logothetis DE. 2012. Dual regulation of voltage-sensitive ion channels by PIP_2. *Frontiers in Pharmacology* **3**: 170-170. DOI:10.3389/fphar.2012.00170, PMID: 23055973.

Roepke TA, Bosch MA, Rick EA, Lee B, Wagner EJ, Seidlova-Wuttke D, Wuttke W, Scanlan TS, Rønnekleiv OK, & Kelly MJ. 2010. Contribution of a membrane estrogen receptor to the estrogenic regulation of body temperature and energy homeostasis. *Endocrinology* **151**: 4926-4937. DOI:10.1210/en.2010-0573, PMID: 20685867.

Rønnekleiv OK, Qiu J, & Kelly MJ. 2019. Arcuate Kisspeptin Neurons Coordinate Reproductive Activities with Metabolism. *Seminars in Reproductive Medicine* **37**: 131-140. DOI:10.1055/s-0039-3400251, PMID: 31869841.

Ruka KA, Burger LL, & Moenter SM. 2013. Regulation of arcuate neurons coexpressing kisspeptin, neurokinin B, and dynorphin by modulators of neurokinin 3 and κ-opioid receptors in adult male mice. *Endocrinology* **154**: 2761-2771. DOI:10.1210/en.2013-1268, PMID: 23744642.

Ryu C, Jang DC, Jung D, Kim YG, Shim HG, Ryu H-H, Lee Y-S, Linden DJ, Worley PF, & Kim SJ. 2017. STIM1 regulates somatic Ca^{2+} signals and intrinsic firing properties of cerebellar Purkinje neurons. *The Journal of Neuroscience* **37**: 8876. DOI:10.1523/JNEUROSCI.3973-16.2017, PMID: 28821659.

Salido GM, Jardin I, & Rosado JA. 2011. The TRPC ion channels: association with Orai1 and STIM1 proteins and participation in capacitative and non-capacitative calcium entry. *Advances in Experimental Medicine and Biology* **704**: 413-433. DOI:10.1007/978-94-007-0265-3_23, PMID: 21290309.

Sliwowska JH, Fergani C, Gawalek M, Skowronska B, Fichna P, & Lehman MN. 2014. Insulin: its role in the

central control of reproduction. *Physiology & Behavior* **133**: 197-206. DOI:10.1016/j.physbeh.2014.05.021, PMID: 24874777.

Smith AW, Bosch MA, Wagner EJ, Rønnekleiv OK, & Kelly MJ. 2013. The membrane estrogen receptor ligand STX rapidly enhances GABAergic signaling in NPY/AgRP neurons: Role in mediating the anorexigenic effects of 17β-estradiol. *American Journal of Physiology: Endocrinology and Metabolism* **305**: E632-E640. DOI:10.1152/ajpendo.00281.2013, PMID: 23820624.

Somasundaram A, Shum AK, McBride HJ, Kessler JA, Feske S, Miller RJ, & Prakriya M. 2014. Store-Operated CRAC Channels Regulate Gene Expression and Proliferation in Neural Progenitor Cells. *The Journal of Neuroscience* **34**: 9107-9123. DOI:10.1523/jneurosci.0263-14.2014, PMID: 24990931.

Song WJ, Mondal P, Wolfe A, Alonso LC, Stamateris R, Ong BW, Lim OC, Yang KS, Radovick S, Novaira HJ, Farber EA, Farber CR, Turner SD, & Hussain MA. 2014. Glucagon regulates hepatic kisspeptin to impair insulin secretion. *Cell Metabolism* **19**: 667-681. DOI:10.1016/j.cmet.2014.03.005, PMID: 24703698.

Stincic TL, Rønnekleiv OK, & Kelly MJ. 2019. Membrane and nuclear initiated estrogenic regulation of homeostasis. *Steroids*: 108428. DOI:10.1016/j.steroids.2019.108428, PMID: 31229508.

Sun Y, Zhang H, Selvaraj S, Sukumaran P, Lei S, Birnbaumer L, & Singh BB. 2017. Inhibition of L-Type Ca^{2+} channels by TRPC1-STIM1 complex is essential for the protection of dopaminergic neurons. *The Journal of Neuroscience* **37**: 3364-3377. DOI:10.1523/JNEUROSCI.3010-16.2017, PMID: 28258168.

Tolson KP, Garcia C, Yen S, Simonds S, Stefanidis A, Lawrence A, Smith JT, & Kauffman AS. 2014. Impaired kisspeptin signaling decreases metabolism and promotes glucose intolerance and obesity. *Journal of Clinical Investigation* **124**: 3075-3079. DOI:10.1172/JCI71075, PMID: 24937427.

Wang H, Cheng X, Tian J, Xiao Y, Tian T, Xu F, Hong X, & Zhu MX. 2020. TRPC channels: Structure, function, regulation and recent advances in small molecular probes. *Pharmacology & Therapeutics*: 107497. DOI:10.1016/j.pharmthera.2020.107497, PMID: 32004513.

Wang Y, Deng X, Mancarella S, Hendron E, Eguchi S, Soboloff J, Tang XD, & Gill DL. 2010. The calcium store sensor, STIM1, reciprocally controls Orai and $Ca_V1.2$ channels. *Science* **330**: 105-109. DOI:10.1126/science.1191086, PMID: 20929813.

Wei Q, Krolewski DM, Moore S, Kumar V, Li F, Martin B, Tomer R, Murphy GG, Deisseroth K, Watson SJ, & Akil H. 2018. Uneven balance of power between hypothalamic peptidergic neurons in the control of feeding. *Proceedings of the National Academy of Sciences* **115**: E9489-E9498. DOI:10.1073/pnas.1802237115, PMID: 30224492.

Wilson RC, Kesner JS, Kaufman J-M, Uemura T, Akema T, & Knobil E. 1984. Central electrophysiological correlates of pulsatile luteinizing hormone secretion in the Rhesus monkey. *Neuroendocrinology* **39**: 256-260. DOI:10.1159/000123988, PMID: 6504270.

Xu AW, Kaelin CB, Takeda K, Akira S, Schwartz MW, & Barsh GS. 2005. PI3K integrates the action of insulin and leptin on hypothalamic neurons. *Journal of Clinical Investigation* **115**: 951-958. DOI:10.1172/JCI24301, PMID: 15761497.

Yuan JP, Zeng W, Huang GN, Worley PF, & Muallem S. 2007. STIM1 heteromultimerizes TRPC channels to determine their function as store-operated channels. *Nature Cell Biology* **9**: 636-645. DOI:10.1038/ncb1590, PMID: 17486119.

Zhang C, Bosch MA, Rønnekleiv OK, & Kelly MJ. 2013. Kisspeptin activation of TRPC4 channels in female GnRH neurons requires PIP_2 depletion and cSrc kinase activation. *Endocrinology* **154**: 2772-2783. DOI:10.1210/en.2013-1180, PMID: 23744639.

Zhang C, Roepke TA, Kelly MJ, & Rønnekleiv OK. 2008. Kisspeptin depolarizes gonadotropin-releasing hormone neurons through activation of TRPC-like cationic channels. *The Journal of Neuroscience* **28**: 4423-4434. DOI:10.1523/JNEUROSCI.5352-07.2008, PMID: 18434521.

Zhang C, Tonsfeldt KJ, Qiu J, Bosch MA, Kobayashi K, Steiner RA, Kelly MJ, & Rønnekleiv OK. 2013. Molecular mechanisms that drive estradiol-dependent burst firing of Kiss1 neurons in the rostral periventricular preoptic area. *American Journal of Physiology: Endocrinology and Metabolism* **305**: E1384-E1397. DOI:10.1152/ajpendo.00406.2013, PMID: 24105416.

Figures and Legends

FIGURE 1

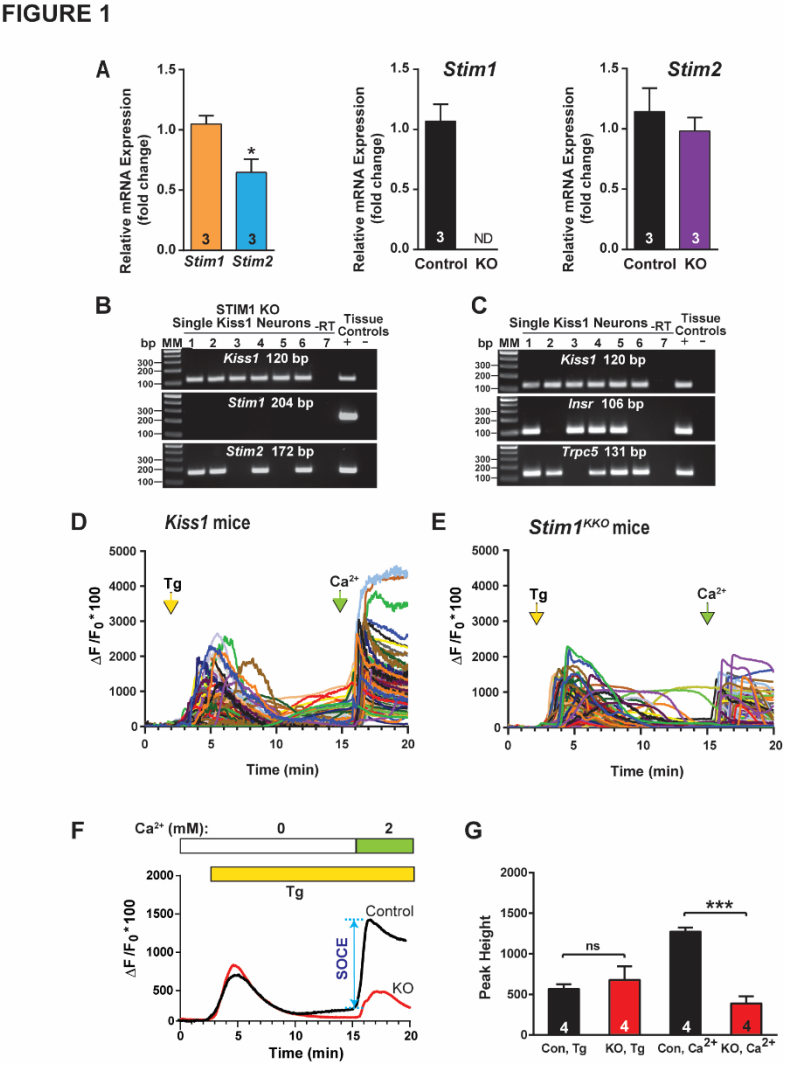

Figure 1. Expression Patterns of *Stim1 and 2* in the arcuate Kiss1 neurons. **A**, quantitative PCR assay measuring *Stim1* and *Stim2* in Kiss1^{ARH} neuronal pools (n = 3 animals, 10 cells in each pool, 4 pools/animal) from *Kiss1*^{Cre} control and *Stim1*^{kko} female mice (n=3 animals per group). Comparison between *Stim1* and *Stim2* in controls only. Bar graphs represent mean ± SEM (Unpaired *t*-test for the left, $t_{(4)} = 3.079$, * $p < 0.05$; For the middle, *Stim1* was non-detectable (ND) in the STIM1^{KKO} neuronal pools; Unpaired *t*-test for the right, $t_{(4)} = 0.7143$, $p = 0.5145$). **B** and **C**, representative gels illustrating mRNA expression of *Stim1* and *Stim2* in single Kiss1^{ARH} neurons from *Stim1*^{kko} mice (**B**) and insulin receptor (*Insr)*, and *Trpc5* subunit expression in single Kiss1^{ARH} neurons from *Kiss1*^{Cre} mice (**C**). The expected base pair (bp) sizes are *Kiss1*, 120 bp; Stim1, 204 bp; Stim2, 172

bp; *Insr*, 106 bp and *Trpc5*, 131 bp. A single neuron was processed without reverse transcriptase (-RT) and RNA extracted from hypothalamic tissue was used as positive (+, with RT) and negative (-, without RT) tissue controls. MM, molecular marker. **D** and **E**, representative traces of GCaMP6s activity based on cytosolic Ca^{2+} measurements in $Kiss1^{ARH}$ neurons from *Kiss1^{Cre}:GCaMP6s* mice (D) and *Stim1^{kko}:GCaMP6s* mice (E). ER Ca^{2+} stores were depleted with 2 µM thapsgargin, a SERCA inhibitor, after 20 min of perfusion with aCSF containing 0 mM Ca^{2+}. SOCE was evaluated by substituting the extracellular aCSF containing 0 mM Ca^{2+} with aCSF containing 2 mM Ca^{2+}. **F**, averaged traces from C and D revealed that deletion of *Stim1* in $Kiss1^{ARH}$ neurons attenuated the store-operated Ca^{2+} entry (SOCE). **G**, bar graphs summarizing the effects of depletion of Ca^{2+} store by Tg and Ca^{2+} influx (SOCE) in $Kiss1^{ARH}$ neurons from Kiss1Cre:GCaMP6s and $Stim1^{kko}$:GCaMP6s mice (unpaired t-test, $t_{(6)} = 0.6372$, p = 0.5475 for depletion of Ca^{2+} store; Unpaired t-test, $t_{(6)} = 8.921$, ***$p = 0.0001$ for SOCE).

FIGURE 2

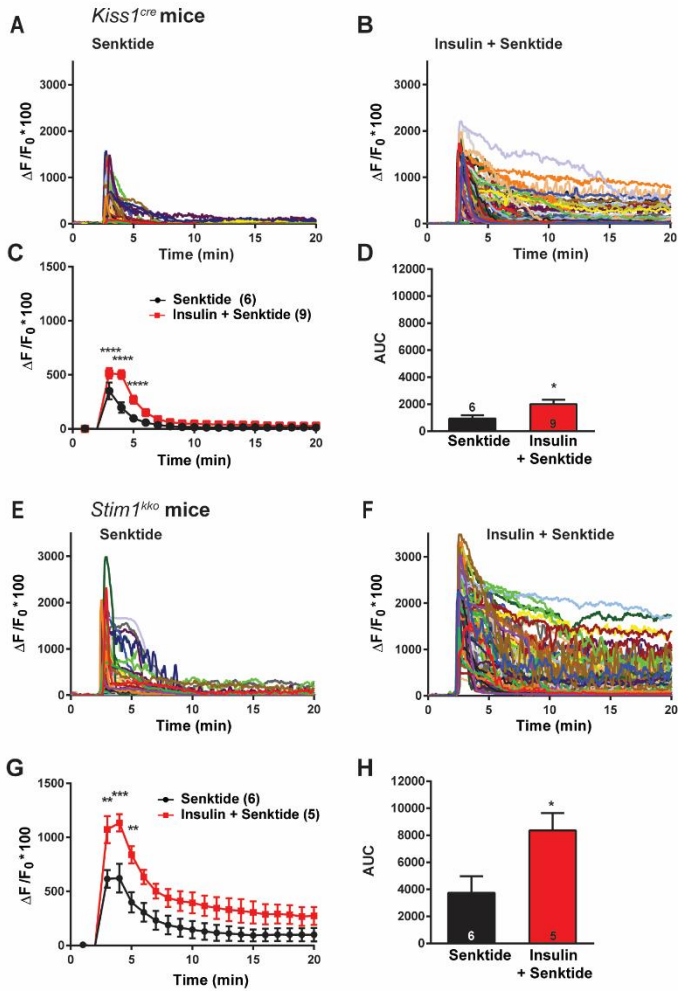

Figure 2. Senktide-induced increase in $[Ca^{2+}]_i$ is augmented by deletion of *Stim1* and further potentiated by insulin in GCaMP6s-expressing $Kiss1^{ARH}$ neurons from *Kiss1* and $Stim1^{kko}$ mice. **A** and **B**, representative traces of senktide-induced $[Ca^{2+}]_i$ in the presence or absence of insulin. Traces represent individual cells within a single slice. **C**, summary of the potentiation of senktide-induced $[Ca^{2+}]_i$ after bath-applied insulin for 18 minutes. Two-way ANOVA: main effect of treatment ($F_{(1,13)} = 5.673$, $p = 0.0332$), main effect of time ($F_{(19,247)} = 82.29$, $p < 0.0001$) and interaction ($F_{(19,247)} = 8.725$, $p < 0.0001$); n = number of slices; *post hoc* Bonferroni test, ****$p < 0.001$. **D**, relative AUC of $Kiss1^{ARH}$ neurons from C. There was a significant difference (Unpaired *t*-test, $t_{(13)} = 2.395$, *$p = 0.0324$) between the groups. **E** and **F**, representative traces of senktide-induced $[Ca^{2+}]_i$ in the presence or absence of insulin in $Kiss1^{ARH}$ neurons from $Stim1^{kko}$ mice. **G**, summary of the potentiation of senktide-induced $[Ca^{2+}]_i$ after bath-applied insulin (20 nM) for 18 minutes in $Kiss1^{ARH}$ neurons

from *Stim1*^{kko} mice. Two-way ANOVA: main effect of treatment ($F_{(1,9)}$ = 6.575, p = 0.0305) , main effect of time ($F_{(19,171)}$ = 48.44, p < 0.0001) and interaction ($F_{(19,171)}$ = 3.548, p < 0.0001); *post hoc* Bonferroni test, **p < 0.01 and *** p < 0.005. **H**, relative AUC of Kiss1^{ARH} neurons from G (unpaired t-test, $t_{(9)}$ = 2.586, *p = 0.0294).

Supplemental video 1. Neurokinin B receptor agonist senktide induces $[Ca^{2+}]_i$ increase in Kiss1^{ARH} neurons expressing GCaMP6s. Imaging of transient Ca^{2+} changes in an arcuate slice using spinning disk confocal microscopy. Fluorescence intensity was measured over 20 minutes, before and after application of senktide (1 µM).

FIGURE 3

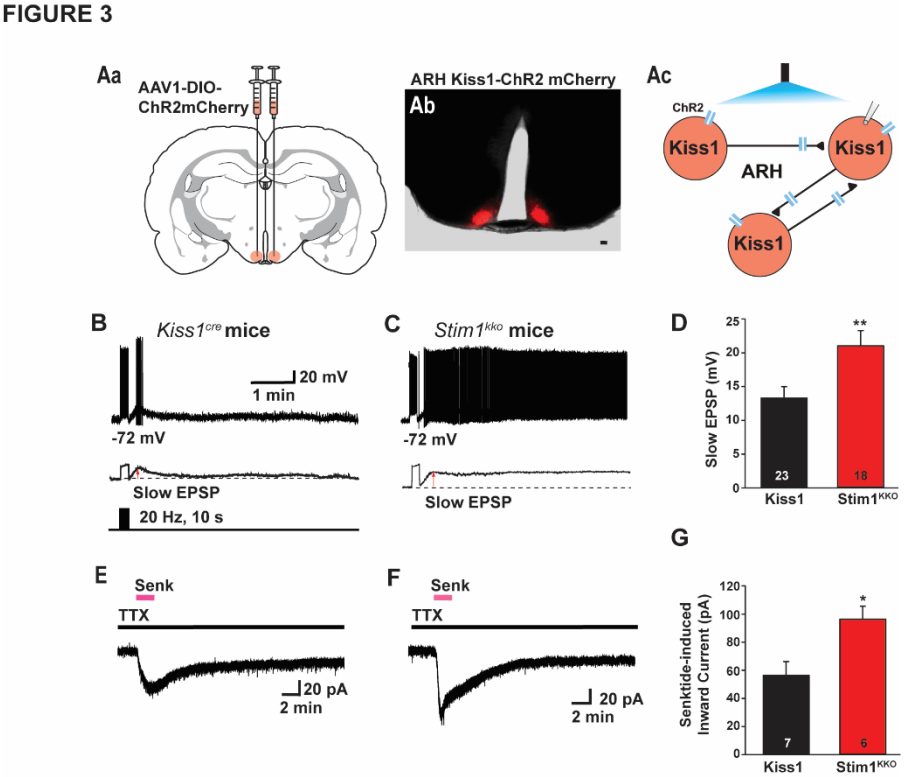

Figure 3. Deletion of *Stim1* augments high-frequency optogenetic stimulation-induced slow EPSP and senktide-induced depolarization in Kiss1^{ARH} neurons. Aa, schematic of a coronal section showing the bilateral viral injections in the ARH with AAV-DIO-ChR2:mCherry. **Ab**, photomicrographs showing coronal sections confirming targeted bilateral injections of DIO-ChR2: mCherry into the arcuate. **Ac**, Experimental protocol: high-frequency photostimulation of Kiss1^{ARH} neurons/terminals and recording of Kiss1^{ARH} neurons. Scale bars, 200 µm for Ab. **B,C**, high-frequency optogenetic stimulation (20 Hz, 10 s) generated slow EPSPs in

a ChR2-expressing Kiss1^{ARH} neuron from control *Kiss1* mice (**B**) and in a ChR2-expressing Kiss1^{ARH} neuron from *Stim1*^{kko} mice (**C**). The lower trace shows the slow EPSP after low-pass filtering from B and C (arrow), respectively. **D**, summary of the effects of *Stim1* deletion on the slow EPSP amplitude. Bar graphs represent the mean ± SEM (Unpaired *t*-test, $t_{(39)}$ = 2.802, ***p* = 0.0079). **E** and **F,** rapid bath application of senktide (1 µM) induced an inward current in the presence of fast sodium channel blockade (TTX, 1µM) in Kiss1^{ARH} neurons from *Kiss1*^{Cre} and *Stim1*^{kko} mice. V_{hold} = - 60 mV. **G**, summary of the effects of senktide in Kiss1^{ARH} neurons from *Kiss1*^{Cre} and *Stim1*^{kko} mice (Unpaired *t*-test, $t_{(11)}$ = 2.929, **p* = 0.0137). Data points represent the mean ± SEM. Cell numbers are indicated.

Supplemental Video 2. High frequency photo-stimulation induces a slow excitatory postsynaptic potential (slow EPSP). Slow EPSP was induced by a 10-s 20 Hz photostimulation (light intensity 0.9 mW and pulse duration, 10 ms) in a ChR2-expressing Kiss1^{ARH} neuron in a slice from a *Kiss1*^{Cre}*::Ai32* mouse.

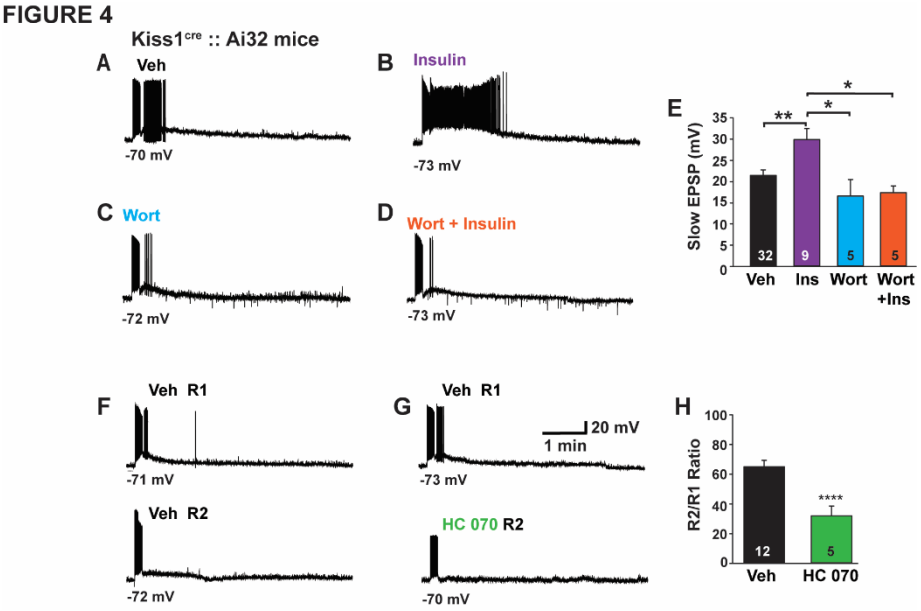

Figure 4. Insulin augments the slow EPSP in Kiss1^{ARH} neurons from *Kiss1*^{Cre}*::Ai32* mice in a PI3K dependent manner and senktide-induced depolarization is antagonized by TRPC5 channel blockers. A–D, representative traces of the slow EPSPs in the presence or absence of PI3 kinase inhibitor wortmannin (100 nM) or insulin (20 nM). **E**, summary of the effects of wortmannin on the insulin-potentiated slow EPSP. The PI3

kinase blocker was applied for 15 min before the application of insulin (20 nM). Comparisons between different treatments were assessed using a one-way ANOVA ($F_{(3, 47)} = 5.0301$, $p < 0.0042$) and the Newman-Keuls's *post hoc* test. **$p < 0.01$, Veh *versus* Ins; *$p < 0.05$, Ins *versus* Wort or Wort + Ins. **F–G,** representative traces of high-frequency optogenetic stimulation-induced slow EPSPs in the presence or absence of TRPC4/5 channel blocker HC 070 (100 nM). **H**, summary of the effects of HC 070 on the slow EPSP (Un-paired t-test, $t_{(15)} = 4.122$, ****$p = 0.0009$).

FIGURE 5

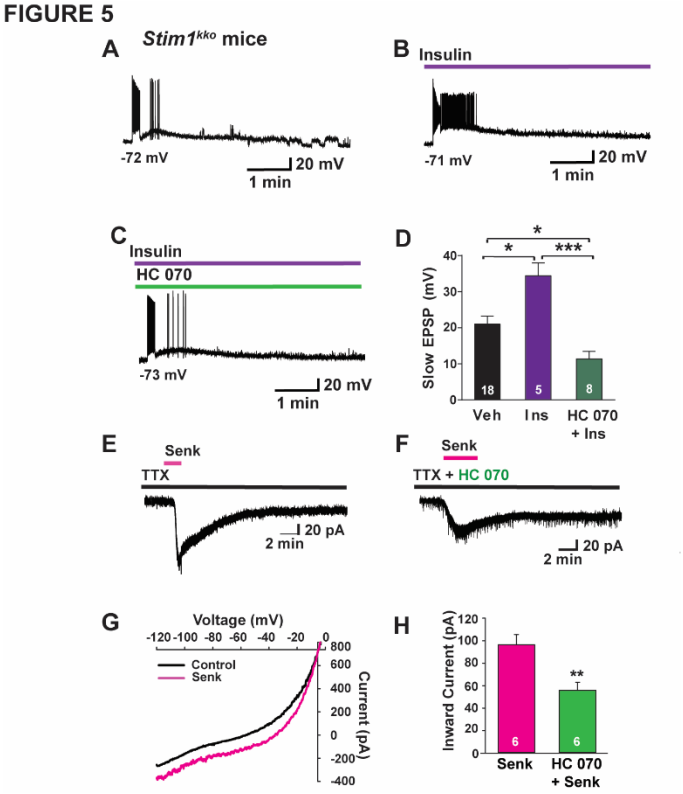

Figure 5. Insulin augments the effects of *Stim1* deletion on the slow EPSP and the senktide-induced depolarization is antagonized by the TRPC5 channel blocker HC 070. A and **B**, representative traces of the slow EPSP in the presence or absence of insulin (20 nM) in ChR2-expressing $Kiss1^{ARH}$ neurons from $Stim1^{kko}$ mice. **C**, a representative trace of the slow EPSP in the presence of selective TRPC5 channel blocker HC 070 (100 nM) and insulin in a ChR2-expressing $Kiss1^{ARH}$ neuron from $Stim1^{kko}$ mice. **D**, summary of the effects of insulin applied for 20 min before high-frequency optogenetic stimulation in the presence or absence of the TRPC5 channel blocker HC 070 (100 nM) on slow EPSPs. Comparisons between different treatments were

assessed using a one-way ANOVA ($F_{(2, 28)}$ = 11.16, p = 0.0003) and the Newman-Keuls's *post hoc* test. ***p < 0.005, Ins *versus* HC 070+Ins; *p < 0.05, Veh *versus* Ins or HC 070+Ins. **E–F,** representative traces of senktide-induced inward current in *Stim1*^{kko} neurons perfused with TTX (1 µM) in the presence or absence of TRPC4/5 blocker HC 070. **G**, the I-V relationship before and during the peak response from the same cell in E indicated that the reversal potential of the nonselective cation current was ~ -10 mV. **H**, summary of the effects of HC 070 on the senktide-induced inward current (Un-paired t-test, $t_{(10)}$ = 3.457, **p = 0.0062). Data points represent the mean ± SEM. Cell numbers are indicated.

FIGURE 6

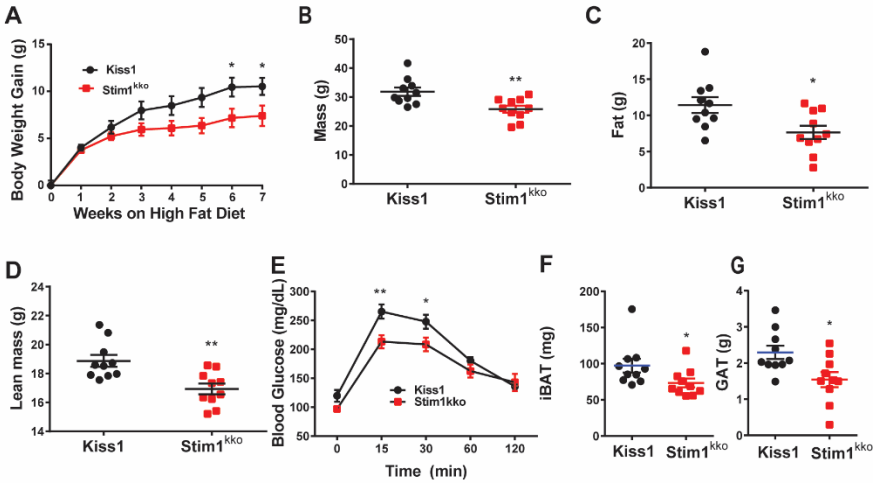

Figure 6. Ablation of Stim1 in Kiss1 neurons attenuates body mass, fat, and lean in mice on a high fat diet. *Stim1*^{kko} and *Kiss1*^{Cre} littermate control females were ovariectomized and fed a high fat diet (HFD; 45% kcal from fat) for seven weeks. **A**, body-weight gain measured once a week for seven weeks. The high fat diet caused significant weight gain in both groups relative to their baseline with the *Kiss1*^{Cre} females gaining significantly weight more by 6 weeks [two-way ANOVA: main effect of treatment ($F_{(1, 18)}$ = 3.839, p = 0.0657), main effect of time ($F_{(7, 126)}$ = 98.07, p < 0.0001) and interaction ($F_{(7, 126)}$ = 4.645, p = 0.0001); Kiss1 control, n = 10, Stim1^{kko}, n = 10; *post hoc* Bonferroni test, *p < 0.05]. **B-D**, mass (B), total body fat (C) and lean mass (D) measured by an EchoMRI Whole Body Composition Analyzer. Lean mass does not include bone and fluids within organs. The difference in mass (B), body fat (C) and lean mass (D) between the groups was significantly different by 6 weeks

on high fat diet (unpaired, two-tailed t-test for B, $t_{(18)}$ = 3.222, **p = 0.0047; unpaired two-tailed t test for C, $t_{(18)}$ = 2.662, *p = 0.0159; unpaired, two-tailed t test for D, $t_{(18)}$ = 3.489, *p = 0.0026). **E**, six weeks after high fat diet, there was a significant difference in GTTs between the two groups (two-way ANOVA: main effect of treatment ($F_{(1, 9)}$ = 6.282, p = 0.0335), main effect of time ($F_{(4, 36)}$ = 88.01, p < 0.0001) and interaction ($F_{(4, 36)}$ = 3.527, p = 0.0158); *Kiss1*^{Cre}, n = 6, *Stim1*^{kko}, n = 5; *post hoc* Bonferroni test, **p < 0.01, *p < 0.05). **F** and **G**, both interscapular brown adipose tissue (iBAT) and perigonadal adipose tissue (GAT) mass of *Stim1*^{kko} were lighter than that of *Kiss1*^{Cre} mice on a fat diet after eight weeks (unpaired, two-tailed t test for iBAT, $t_{(18)}$ = 2.127, *p = 0.0475; unpaired two-tailed t-test for GAT, $t_{(18)}$ = 2.711, *p = 0.0143).

FIGURE 7

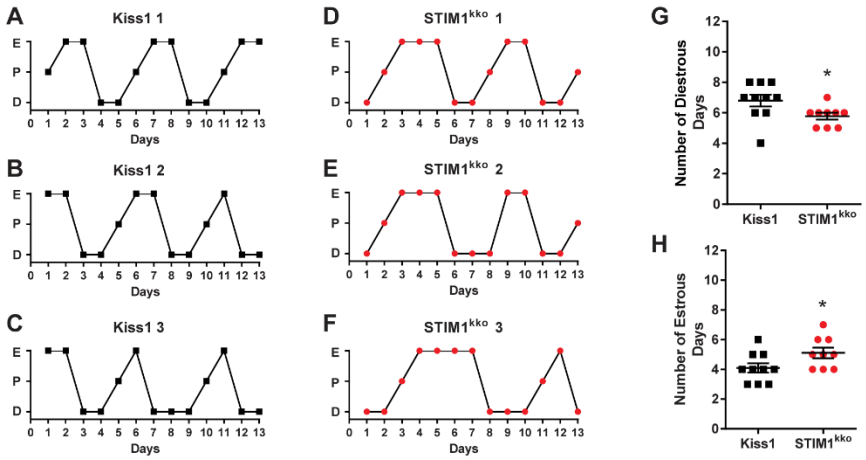

Figure 7. *Stim1*^{kko} mice exhibit more estrous days. **A-F**, representative estrous cycle data from three representative control *Kiss1*^{Cre} and three *Stim1* ^{kko} mice over a thirteen-day period. Vaginal lavage was done daily at 0930 h, and cell cytology was observed and recorded as Diestrus (D), Proestrus (P) or Estrus (E). Summary data for the number of Diestrous days (**G**) and Estrous days (**H**) during the 13 day period was compared between *Kiss1*^{Cre} (n = 10) and *Stim1* ^{kko} mice (n = 9) (unpaired, two-tailed t test for G, $t_{(17)}$ = 2.215, *p = 0.0407; unpaired two-tailed t-test for H, $t_{(17)}$ = 2.151, *p = 0.0461).

FIGURE 8

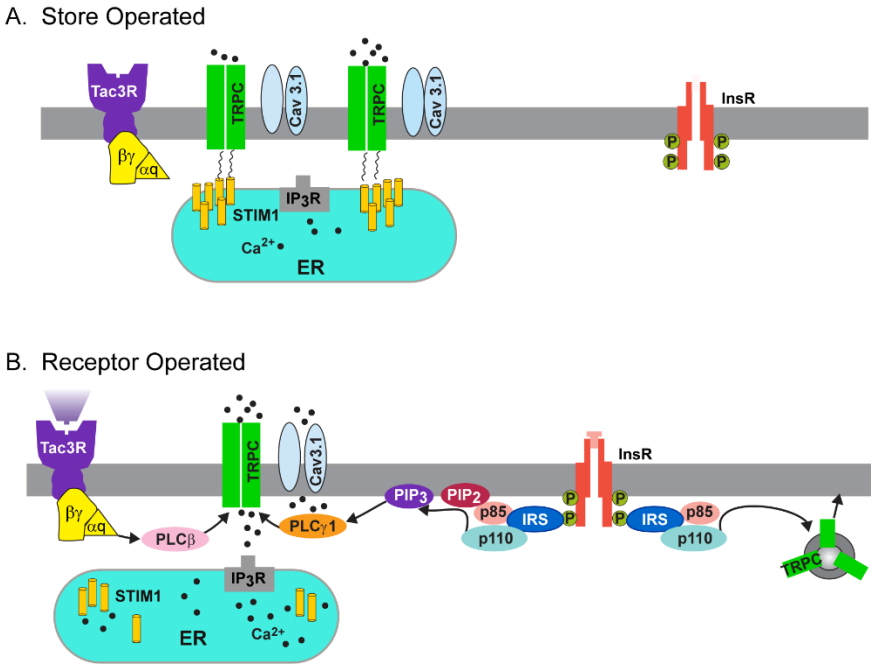

Figure 8. A cellular model of insulin and NKB activation of TRPC5 channels in Kiss1^{ARH} neurons. A, under physiological stress and in the absence of E_2, stromal interaction molecule 1 (STIM1) interacts with TPRC5 channels thereby engaging these Ca^{2+} channels as store-operated channels, which are activated with endoplasmic reticulum (ER) depletion of Ca^{2+}. **B**, however, under physiological conditions in reproductively active females, E_2 down-regulates the expression of STIM1, thereby converting the TRPC5 channels to receptor-operated channels in Kiss1^{ARH} neurons. Insulin signals via InsR-IRS-PI3K-PLCγ1 to activate TRPC5 channels, generating a robust inward Na^+/Ca^{2+} current to depolarize Kiss1^{ARH} neurons, activating T-type calcium (Cav3.1) channels to greatly increase Kiss1^{ARH} neuronal excitability. PI3K (p85/p110) will also accelerate the rapid insertion of TPRC5 channels into the plasma membrane (Bezzerides et al., 2004), which underlies the insulin augmentation of the excitatory effects of NKB in Kiss1^{ARH} neurons. Neurokinin B (NKB) binds to its receptor (Tac3R) to activate Gαq – PLCβ signaling cascade to facilitateTPRC5 channels opening.

Table 1. Primer Table

Gene Name (encodes for)	Accession Number	Primer Location (bp)	Product Length (bp)	Annealing Temp (°C)	Efficiency Slope	Efficiency r^2	Efficiency %
Kiss1 (Kiss1)[a,b]	NM_178260	64-80 (exon 1)	120	57[a], 60[b]	-3.410	0.989	97
		167-183 (exon 2)					
Stim1 (STIM1)[a]	NM_009287	797-816 (exon 2)	204	59			
		981-1000 (exon 3)					
Stim1 (STIM1)[b]	NM_009287	821-839 (exon 2)	135	60	-3.311	0.977	100
		937-955 (exon 3)					
Stim2 (STIM2)[a]	NM_001363348	620-638 (exon 2)	172	59			
		773-791 (exon 4)					
Stim2 (STIM2)[b]	NM_001363348	1784-1803 (exon 11)	131	60	-3.439	0.993	95
		1895-1914 (exon 12)					
Gapdh (GAPDH)[b]	NM_008084	689-706 (exon 4)	93	60	-3.352	0.998	99
		764-781 (exon 5)					
Insr (IR)[a]	NM_001330056	3649-3668 (exon 17)	172	61			
		3733-3754 (exon 18)					
Trpc5 (TRPC5)[a]	NM_009428	2206-2227 (exon 6)	131	63			
		2315-2336 (exon 7)					

[a]primers for scRT-PCR.
[b]primers for qPCR.